Engineered Science
DOI: https://dx.doi.org/10.30919/es8e788

The Effects of Dielectric and Thermal Property Functions on The Thermal Response during the Focused Microwave Ablation Treatment in the Liver Cancer Model: Numerical Investigation

Wutipong Preechaphonkul and Phadungsak Rattanadecho*

Abstract

Microwave ablation (MWA) is a minimally invasive cancer treatment technique using microwave power to create thermal damage in the local malignant tumor by using a microwave antenna. In the previous literature, there are investigated some property sensitivity but used by supposed values and supposed situations. So, this study has investigated the sensitivity of property functions based on a realistic situation that is a different point from the literature, which considered sensitivity by supposed value. This study investigated the effect of widely properties model types on the thermal response of liver tissue during the MWA treatment process. The mathematical models are developed coupled with electromagnetic wave propagation, bioheat, and Arrhenius damage equations to describe the specific absorption rate (SAR) and temperature distribution in the tissue during MWA process. In particular, the results calculated from models with different property model types are investigated and demonstrated with the same conditions, as well as the experimental results from previous work in order to show the validity of the numerical results. This study presented the sensitivity of the individual property functions as the relative permittivity, electrical conductivity, blood perfusion rate, thermal conductivity, and specific heat capacity of the liver tissue to indicate the high property functions that should be considered as a function depending on the temperature. The results show that the difference in SAR and temperature distribution area appears within the liver when using different model types in the same conditions. The electrical conductivity is the most impact function. However, the difference between the various models can be observed when tissue temperature exceeds 60 ºC, and it is clearly observed when tissue temperature exceeds 100 ºC. The main reason for the difference is that some functions consider the effect of tissue evaporation during the ablation process, but some properties are not considered.

Keywords: Microwave ablation (MWA); Dielectric properties; Thermal properties; Sensitivity property functions; Heat transfer; Numerical investigation.
Received: 13 July 2022; Revised: 01 November 2022; Accepted: 07 November 2022.
Article type: Research article.

1. Introduction

Hepatocellular carcinoma (HCC) is common cancer and one of the leading causes of death worldwide. Hepatocellular carcinoma (HCC) is common cancer and one of the leading causes of death worldwide. Unfortunately, although HCC is common cancer, 40% of patients with HCC cannot be accessible to surgery, which is a mainstay curative treatment for the early stage of HCC.[1,2] Thus, the local alternative medicine, such as radiofrequency ablation (RFA) and microwave ablation (MWA), are widely used in the early-stage HCC therapeutic.[3]

MWA is a minimally invasive cancer treatment technique using microwave power to create thermal damage in the local malignant tumor. The microwave antenna is inserted into the local malignant tumor to transmit microwave energy in the treatment process. The microwave is absorbed and converts the internal heat in the tumor. This treatment aims to create thermal damage in the tumor area without damage to the surrounding healthy tissue.[4,5]

Although MWA indicated operation for early-stage HCC

Center of Excellence in Electromagnetic Energy Utilization in Engineering (CEEE), Department of Mechanical Engineering, Faculty of Engineering, Thammasat School of Engineering, Thammasat University (Rangsit Campus), Pathumthani 12120, Thailand.
**Email:* ratphadu@engr.tu.ac.th (P. Rattanadecho)

in Barcelona Clinic Liver Cancer,[6] incorrect conditions during MWA treatment could be created injury to patients, such as the heat spread out over the boundaries of the malignant tumor area. Therefore, the MWA for early-stage HCC studies is necessary to investigate. It could not apply to human liver beings due to being unethical. Many researchers have been experimental studies with animals.[7-14] However, the experimental studies with the animals had limitations, and it is not nearly realistic human liver. Thus, the numerical simulation is used to demonstrate the phenomenon in the human liver during the MWA treatment process. It has been the advantage of needing only a short period, the low economic cost, humanity, and could be set up with conditions near to those of a natural human liver.

Several studies have proposed mathematical models for predicting phenomena in the liver tissue during the MWA treatment process.[5,15,16] Many concepts, such as the bioheat approach, the porous media approach, and the tissue deformation approach, have been applied to develop high accuracy models. In 2007, Yang *et al.* proposed a modified bioheat model for predicting the temperature distribution in the liver during the MWA treatment process.[15] This model was considered the tissue evaporation term and presented the remaining water content in the tissue during the ablation process. Later, Keangin *et al*. developed the predicting model with considered tissue deformation.[5] Rattanadecho and Keangin proposed the numerical modeling of heat transfer in the liver tissue during MWA treatment based on porous media theory.[16] However, developing the mathematical model by modifying governing equations or a new computational approach might not be the best way to develop a highly accurate model. In numerical computation, the accuracy of tissue properties is quite essential to the results.

Most previous studies were assumed the tissue properties to a constant value to reduce the complexity of the problem or lack of information. Recent liver cancer studies with the MWA treatment have used the more appropriate properties for the actual situation. Such as, Wang *et al*. studied the MWA treatment effectiveness by using a multi-slot antenna.[17] The dielectric properties and thermophysical properties of tissue were assumed to depend on the temperature in this study. The dielectric properties functions based on the Keangin *et al*. study and Brace study.[6,18] The thermophysical properties, such as thermal conductivity, specific heat capacity, and density, were developed based on Yang *et al*. study,[15] which considered the remaining water content in the tissue during the ablation process. Later, Shao *et al.* proposed the nano-assisted in irregularly-shaped liver tumors with radiofrequency ablation treatment (RFA).[19] In this study, thermal properties were considered as piecewise functions that depended on the tissue temperature, such as the thermal conductivity based on the Trujillo and Berjano study,[20] the specific heat capacity based on Dos Santos *et al*. study.[21] Especially, this study applied the blood perfusion rate depending on the degree of tissue injury during the ablation process. Later, Xu *et al.* proposed the study of an optimal aperiodic tri-slot coaxial antenna with the π-matching network section in MWA treatment.[22] In this study, the dielectric properties were developed as same as in the Wang *et al*. study, but the electrical conductivity during high tissue temperature was based on Z. Ji and Brace's study.[23] In thermophysical properties of the tissue, this study used concepts that the properties will depend on the tissue temperature in a specific range of the tissue temperature, and after that, properties will be constant—these concepts as the same as the Shao *et al.* study.

During the MWA treatment process, the liver tissue properties are the same properties in the same treatment situation. Thus, the property functions should get the property values in the same direction, but there were many concepts and various values for tissue properties during the MWA treatment. Therefore, a study should investigate and demonstrate the effectiveness of various function properties systematically. In the previous study, the sensitivity of the tissue properties during thermal ablation treatment could be observed, particular the sensitivity of the dielectric properties depends on the tissue temperature, such as Brace study,[18] Z. Ji and Brace study,[23], Wu *et al*. study[9] Sebek *et al.* study.[24] Most studies focused on the dielectric properties and proposed that the dielectric function depends on the tissue temperature. However, these studies did not consider the influence of various functions that could affect the thermal response during the MWA process. However, Lopresto *et al*. proposed the effects of tissue properties variations on predictive models for treatment planning.[11] In this study, the high impact properties of the predicting model, such as the relative permittivity, electrical conductivity, specific heat capacity, density, and thermal conductivity, were investigated and considered the effect on the tissue temperature distribution. The results of this study indicated specific properties that could highly affect the thermal response during the MWA treatment process. Although this study investigated the effect of various properties on the thermal response during the MWA treatment process, this study was investigated by adding the same variation in every property. The properties of tissues did not change in the same variation. As the tissue temperature increases to some point, some properties might increase to double value, but some properties might be decreased by 25%. Therefore, the study was not suitable for actual treatment

conditions by adding the same variation in every property.

Furthermore, a comparison of the effect of the difference function in the same properties of liver tissue during the MWA process could not be found in the literature. Thus, this study focused on the thermal response of the liver tissue during the MWA process when using different properties model types and investigated the effect of each properties function by using numerical simulation. In this study, the different properties model types are developed based on the constant properties model,[16,25] Shao *et al*. model,[19] Wang *et al*. model,[17] and Xu *et al*. model.[22] These concepts were used widely in liver cancer treatment with the MWA studies and recent.

This study aims to analyze and demonstrate the effect of properties model types and the characteristics of properties functions on the thermal response in the liver tissue during the MWA process by using numerical simulation. This study focused on the four properties models, which are widely used for the liver cancer treatment with MWA process studies, namely: 1) constant properties model[16,25] 2) Shao *et al*. model,[19] 3) Wang *et al*. model,[17] and 4) Xu *et al*. model.[22] The SAR, temperature, and fraction of necrotic tissue distribution in the liver tissue during the MWA process are obtained by the numerical simulations of the electromagnetic wave propagation, heat transfer, and Arrhenius damage equation. The modeling of the electromagnetic wave propagation coupled with heat transfer in the liver tissue is required to investigate the cited properties model types. Moreover, the characteristics of properties, i.e., relative permittivity, electrical conductivity, and thermophysical properties functions, are compared and investigated the impact on the thermal response in the liver tissue during the MWA process. In this study, the mathematical model is developed based on the electromagnetic wave propagation equations coupled with heat transfer in the biological equation. The system of equations was solved by using the finite elements method (FEM). The accuracy of the numerical model was tested by mesh independent and validation with an experimental study obtained by Yang *et al*..[15] The results presented indicate the influence of each property function on the thermal response of the liver tissue during the MWA process. Furthermore, this study provides the essential aspects for a fundamental understanding of the effects of the properties of function models on the liver during the MWA process under numerical study. The presented results can be used as a guideline for developing the cancer ablation model and the practice of cancer ablation treatment.

2. Problem description

MWA is a minimally invasive cancer treatment technique using the microwave antenna. The microwave antenna is transmitted the microwave energy into the local tumor during the treatment process. The coaxial slot antenna is the standard and popular antenna for MWA applications. Because of its size (small diameter), design simplicity, low cost to manufacture, and convenient adaptation to treatment.[16] This study uses the coaxial single slot antenna to transmit the microwave energy into the tumor for all study cases. The coaxial slot antenna consists of the inner conductor, the outer conductor, dielectric, and catheter (made of polytetrafluorethylene; PTFE),[5] as shown in Fig. 1.[4,5] The dimension and dielectric properties of the coaxial slot antenna are shown in Tables 1-2.[4,5,16] The coaxial slot antenna is operated at 2.45 GHz. In this frequency, many studies indicated a low reflection coefficient that denotes an inefficient state of an antenna. This study investigated the influence of properties model types and the characteristics of properties function on the thermal response in the liver tissue during the MWA process by using numerical simulation.

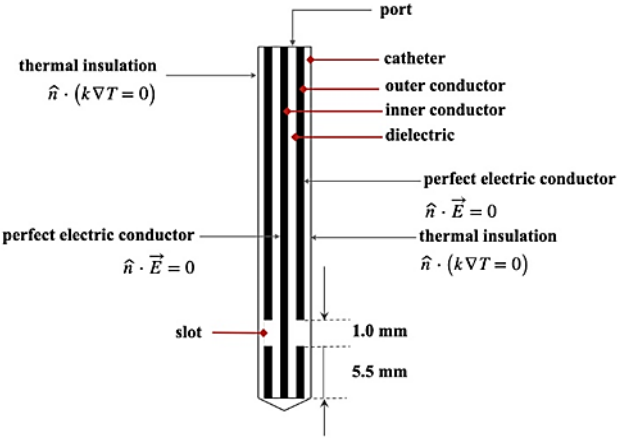

Fig. 1 Model geometry of a microwave coaxial slot antenna.[4,5]

The studies of liver treatment with the MWA process use varying microwave power, starting at 10 W to 140 W. However, the practical treatment and some studies based on experimental are using microwave power in the range of 45W to 60W. To reduce the phenomenon's complexity, this study uses microwave power of 45 W, which is widely used in experimental treatment or numerical modeling.

Table 1. Dimension of a coaxial single slot antenna.[4,5]

Materials	Dimensions (mm)
Inner conductor	0.135 (radial)
Dielectric	0.335 (radial)
Outer conductor	0.460 (radial)
Catheter	0.895 (radial)
Slot	1 (wide)

Table 2. Dielectric properties of coaxial single slot antenna.[4,5,16]

Properties	Relative permittivity, ε_r	Electric conductivity, σ (S/m)	Relative permeability, μ_r
Dielectric	2.03	0	1
Catheter	2.1	0	1
Slot	1	0	1

The model geometry of liver tissue during the MWA process is considered under the axisymmetric assumption, as shown in Fig. 2. The dimension of the model geometry has a radius of 30 mm, and a height of 80 mm, which is suitable for the condition of the natural liver. The coaxial slot antenna is inserted into the liver tissue at 70.5 mm depth. The advantage of the simulation under the axisymmetric assumption is minimized computation time while maintaining good resolution and representing the full three-dimensional result.

The mathematical model is developed under the electromagnetic wave propagation equations coupled with heat transfer in the biological equation. This study is focused on four types of properties models as follows; 1. the constant properties model, 2: Shao *et al*. model,[19] 3. Wang *et al*. model,[17] and 4. Xu *et al*. model.[22] The effect of the properties model types is demonstrated on the SAR, temperature, and fraction of necrotic tissue distribution in the liver tissue during the MWA process. In addition, the characteristics of the dielectric properties and the thermophysical properties are investigated in the temperature distribution in the liver tissue during the MWA process. The effect of characteristics of the dielectric properties and the thermophysical properties are considered under the same model geometry, governing equations, and initial and boundary conditions. In addition, the dimension and properties of the coaxial slot antenna are considered under the same condition in all cases. The material properties of the liver tissue constant properties model are given in Table 3,[16,17,19,22] operated at a frequency of 2.45 GHz.

3. Methods and formulation

A mathematical model has been formulated to predict the electromagnetic wave propagation as well as SAR distribution, temperature distribution, and damaged tissue area in the liver tissue during the MWA process. This section will illustrate an analysis of electromagnetic wave propagation, heat transfer, and damaged tissue in the liver during the MWA process. The system of governing equations and initial and boundary conditions is solved numerically using the FEM. The relevant boundary conditions are described in Fig. 2.

3.1 Electromagnetic wave propagation analysis

In this study, electromagnetic wave analysis is implemented to develop the mathematical model, which is developed to predict the electromagnetic fields and the SAR distribution in the liver tissue during the MWA treatment process. To reduce the complexity of the problem, the following assumptions are made:

(1) The electromagnetic wave propagation is propagated in the two dimensions axisymmetric analysis.

(2) The electromagnetic wave propagation in the coaxial slot antenna is characterized by transverse electromagnetic fields (TEM).[26]

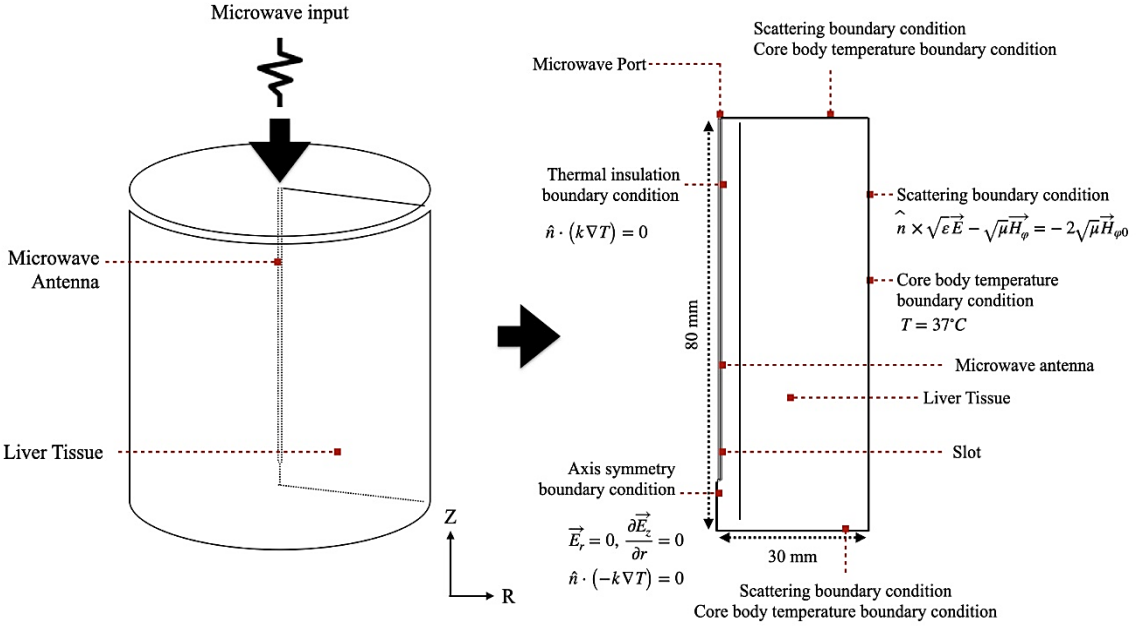

Fig. 2 The model geometry and boundary conditions of liver tissue during the MWA treatment process.

Table 3. The dielectric and thermal properties of liver tissue.

Properties	Constant properties model	Shao *et al.* model	Wang *et al.* model	Xu *et al.* model
Relative permittivity, ε_r	43.00	43.00	$\varepsilon_{r,\,Wang}$ (T)	$\varepsilon_{r,\,Wang}$ (T)
Electric conductivity, σ_{el} (S/m)	1.69	1.69	σ_{Wang} (T)	σ_{Xu} (T)
blood perfusion rate, ω_b (1/s)	0.0036	$\omega_{b,\,Shao}$ (Ω)	$\omega_{b,\,Wang}$ (T)	$\omega_{b,\,Xu}$ (T)
Thermal conductivity, k_{th} (W/mºC)	0.497	k_{Shao} (T)	k_{Wang} (W_a)	k_{Xu} (T)
Density, ρ	1,030	1,030	ρ_{Wang} (W_a)	1,030
Specific heat capacity, Cp (J/kg ºC)	3,600	$C_{p,\,Shao}$ (T)	$C_{p,\,Wang}$ (W_a)	3,600

(3) The electromagnetic wave propagation in the liver tissue is characterized by transverse magnetic fields (TM).[26]

(4) The dielectric properties are assumed to be homogeneous and uniform.

The coaxial slot antenna's wave propagation is considered the transverse electromagnetic field (TEM).[26] The wave propagation is calculated under Maxwell's equations, which mathematically describe the interdependence of the electromagnetic waves. The general form of Maxwell's equations is simplified to demonstrate that the electromagnetic field penetrated the liver tissue, given as.[5,16]

$$\text{Electric field } (\vec{E}) \quad \vec{E} = \vec{e_r}\frac{C}{r}e^{j(\omega t - kz)} \tag{1}$$

$$\text{Magnetic field } (\vec{H}) \quad \vec{H} = \vec{e_\phi}\frac{C}{rZ}e^{j(\omega t - kz)} \tag{2}$$

where $C = \sqrt{\frac{ZP_{in}}{\pi \cdot ln(R_{outer}/R_{inner})}}$ is the arbitrary constant, Z is the wave impedance (Ω), Pin is the microwave power input (W), R_{outer} is the dielectric outer radius (m), R_{inner} is the dielectric inner radius (m), f is the frequency (Hz), $\omega = 2\pi f$ is the angular frequency (rad/s), k is the wave propagation constant (m^{-1}), which relates to the wavelength (λ) in medium: $k = \frac{2\pi}{\lambda}$.

The electromagnetic wave propagation in the liver tissue is considered by the transverse magnetic field (TM),[26] as described by the following equation:

$$\nabla \times \left(\left(\frac{1}{\varepsilon_r} - \frac{j\sigma}{\omega\varepsilon_0}\right)^{-1}\nabla \times \vec{H_\theta}\right) - \mu_r k_0^2 \vec{H_\theta} = 0 \tag{3}$$

where $\vec{H_\theta}$ is magnetic field intensity (A/m), μ_r is relative permeability, ε_r is relative permittivity, $\varepsilon_0 = 8.8542 \times 10^{-12}$ F/m is the permittivity of free space, σ is electric conductivity (S/m), k_0 is the free space wavenumber (m^{-1}), and $\omega = 2\pi f$ is the angular frequency (rad/s).

The interaction of an electromagnetic wave with liver tissue could be defined in terms of a SAR. When the coaxial slot antenna transmits the electromagnetic wave, it passes through it and then propagates throughout the entire domain. The electromagnetic wave is absorbed and converted to heat generation in liver tissue. Thus, SAR represents the microwave power absorption deposited per unit mass in tissue (W/kg).[4,5] The SAR is given by:

$$SAR = \frac{\sigma}{2\rho}\,|\,\vec{E}\,| \tag{4}$$

where σ is the electrical conductivity (S/m), ρ is the tissue density (kg/m3), and $\vec{E}$ is the electric field intensity (V/m). The SAR was converted to the heat generated in the liver tissue (Q_{ext}), which is defined as:

$$Q_{ext} = \frac{\sigma|\vec{E}|^2}{2} = \rho \cdot SAR \tag{5}$$

This study investigated the effect of the property functions sensitivity on the thermal response during the MWA process in the liver cancer model. The four primary property function models are compared under the same governing equations. For the constant properties and Shao *et al*. models, the dielectric properties of liver tissue are used to constant values, as shown in Table 3.[16,17,19,22] For the Wang *et al*. model and Xu *et al*. model, the dielectric properties of liver tissue are considered as functions of temperature; the relative permittivity (ε_r) of the Wang *et al*. and Xu *et al*. models are approximated under the same function. The electric conductivity (σ) of the liver tissue between Wang *et al*. and Xu *et al*. models are considered as different piecewise functions, all the dielectric property functions mentioned above, given in Appendix A.

The boundary conditions of electromagnetic wave analysis are considered under the same conditions for all cases, and the following conditions are made:

1. The top, right, and bottom sides of the liver domain are assumed to be a scattering boundary condition to eliminate the reflections:

$$\hat{n} \times \sqrt{\epsilon}\vec{E} - \sqrt{\mu}\vec{H_\theta} = 2\sqrt{\mu}\vec{H_{\theta 0}} \tag{6}$$

2. The boundary conditions of the inner and outer conductor of the coaxial slot antenna as the perfect electric conductor (PEC) boundary conditions:

$$\hat{n} \times \vec{E} = 0 \quad (7)$$

3. The port boundary condition is assumed at the inlet of the coaxial slot antenna with the microwave power set of 45 W.
4. The electrical symmetry boundary condition is applied at r =0

$$\vec{E_r} = 0 \quad (8a)$$

$$\frac{\partial \vec{E_z}}{\partial r} = 0 \quad (8b)$$

3.2 Heat transfer analysis

In this study, heat transfer analysis is implemented to develop the mathematical model, which predicts the temperature distribution in the liver tissue during the MWA treatment process. The heat transfer analysis is considered only for the liver tissue domain. To reduce the complexity of the problem, the following assumptions are made:

(1) The heat transfer of the liver tissue is considered in the two dimensions axisymmetric analysis under the bioheat approach
(2) The heat transfer analysis is considered only for the liver tissue domain.
(3) The chemical reaction and phase change in the liver tissue are ignored.
(4) The heat transfer of the coaxial slot antenna is ignored.
(5) The liver tissue is assumed to the homogeneous and thermally isotropic.
(6) The thermal properties of the living tissue are uniform.

The heat transfer analysis in the liver tissue can be described by the Pennes bioheat equation,[27] which can be written as follows:

$$\rho C_p \frac{\partial T}{\partial t} = \nabla \cdot k\nabla T + \rho_b C_{p,b} \omega_b (T_b - T) + Q_{met} + Q_{ext} \quad (9)$$

where ρ is the density of living tissue (kg/m^3), C_p is the specific heat capacity of tissue (J/kg.ºC), T is the temperature of living tissue (ºC), k is the thermal conductivity of tissue (W/m.ºC), ρ_b is the destiny of blood (kg/m3), $C_{p,b}$ is the specific heat capacity of blood (J/kg.ºC), ω_b is blood perfusion rate (s^{-1}), Q_{met} is the metabolism heat source (W/m^3) and Q_{ext} is the external heat source term (W/m^3). According to a previous study, Q_{ext} = 33,800 (W/m^3)

This study investigated the effect of the property functions sensitivity on the thermal response during the MWA process in the liver cancer model. The four primary property function models are investigated under the same governing equations as well as the boundary conditions and initial conditions. For the constant properties model, blood perfusion rate and the thermal properties, i.e., thermal conductivity and specific heat capacity of the liver tissue, given in Appendix B.

The boundary conditions of heat transfer analysis are considered under the same conditions for all cases, and the following conditions are made:

1. The top, right, and bottom sides of the liver domain are assumed to be constant with the core body temperature, as shown in Equation (10)

$$T = 37°C \quad (10)$$

2. The interfaces of liver tissue with the coaxial slot antenna are considered insulation thermally.

$$\hat{n} \cdot (k\nabla T) = 0 \quad (11)$$

3. The thermal symmetry boundary condition is applied r=0 for all cases.

$$\hat{n} \cdot (k\nabla T) = 0 \quad (12)$$

3.3 Thermal damaged analysis

The thermal damaged tissue analysis is a subsection of heat transfer analysis. Thus, it is only applied in the liver tissue domain. The thermal damaged tissue analysis follows the assumption of the reduced complexity of the problem.

(1) The thermal damage of the liver tissue is considered in the two dimensions of axisymmetric analysis.
(2) The thermal damaged analysis is considered only for the liver tissue domain.
(3) The thermal damage analysis is caused by thermal treatment.

Thermal damage is the thermal injury of the tissue, for which the injury model proposed by Henriques & Moritz is used, namely the Arrhenius damage equation.[28] The thermal damage in the tissue can be defined as the denaturation of the proteins in the tissue, as follows:

$$\Omega = A\int_0^t exp\left(\frac{-E_a}{RT}\right) dt \quad (13)$$

where Ω(t) is the cumulative tissue damage, A is the frequency factor (s^{-1}), E_a is the activation energy (J/mol), and R is the universal gas constant (J/mol.K). The fraction of necrotic tissue (θ_d) can be expressed as:

$$\theta_d = 1 - exp(-\Omega) \quad (14)$$

4. Calculation procedure

This study investigated the influence of properties model types, and the characteristics of properties function on the thermal response in the liver tissue during the MWA process by numerical simulation. The literature obtains these data,[15-17,19,22] the accuracy of our parameter can be ensured. According to the geometry reference, the model geometry is considered a cylinder with 80 mm in the longitudinal antenna direction and 30 mm in the radial direction.[16,17] as shown in Fig. 2. This

study used the microwave antenna as the coaxial single slot antenna. According to the literature,[5] the dimension of the antenna is shown in Fig. 1. The mathematical model coupled with electromagnetic wave propagation and heat transfer in the biological tissue. The system of equations is solved with FEM by using COMSOL™ Multiphysics to demonstrate the effect of properties model types and the characteristics of properties function in the liver tissue during the MWA process. The computation scheme starts with computing the external heat source by solving the electromagnetic wave propagation equation and subsequently solves the time-dependent temperature at very points under the bioheat equation. However, when the temperature changes would be affected the dielectric and the thermophysical properties of the liver tissue. The models under the variation function properties recalculated the electromagnetic field in the tissue with the updated dielectric properties and thermophysical properties, which affect the external heat source. Therefore, the temperature at every point would be recalculated until the last time step.

In this study, the numerical model for all cases is discretized using triangular elements with Lagrange quadratic shape functions, and the elements are adaptive in sensitive areas. The initial time steps, the maximum time steps, and relative tolerance to solve the transient problem are $1x10^{-3}$ s, 0.1 s, and $1x10^{-2}$, respectively. The convergence test for the liver cancer model shows the relation with the temperature at the sensitive point—the density of elements, approximately 43,893 elements, meshed independently. Increasing the number of elements past this point did not lead to significantly different computational results, as shown in Fig. 3. The maximum element size, minimum element size, and maximum element growth rate are 0.4 mm, 0.0016 mm, and 1.25, respectively, where the verification of the numerical model will be presented in the next section.

5. Results and discussion

This section consists of three-part; Part one shows the verification accuracy of the present model. Part two shows the thermal repose in liver tissue during the MWA process when applied to the different properties model types. In this part, the properties model types consist of the constant properties model, Shao *et al*. model,[19] Wang *et al*. model,[17] and Xu *et al*. model.[22] After that, the last part shows the impact of each property function one by one and comparison with the constant properties model. In this part, the most effective property function on the thermal response in the liver tissue during the MWA process could be indicated.

5.1 Verification of the model

In order to verify the accuracy and precision of the presented numerical model, the simulation result with a coaxial slot antenna is validated against the experimental and numerical results obtained by Yang *et al*.[15] under the same testing condition. In the validation test, the MWA process operated with the microwave power input of 75 W with a frequency of 2.45 GHz, and the initial temperature was set at 8 deg C. In the verification test, the radius of the coaxial antenna is 1.25 mm, inserted 20 mm deep into the liver tissue, and the heating time of 50 s. The verification results show the transient temperature of two points, 4.5 and 9.5 mm away from the microwave coaxial antenna, as shown in Fig. 4. Table 4 shows the RMSE

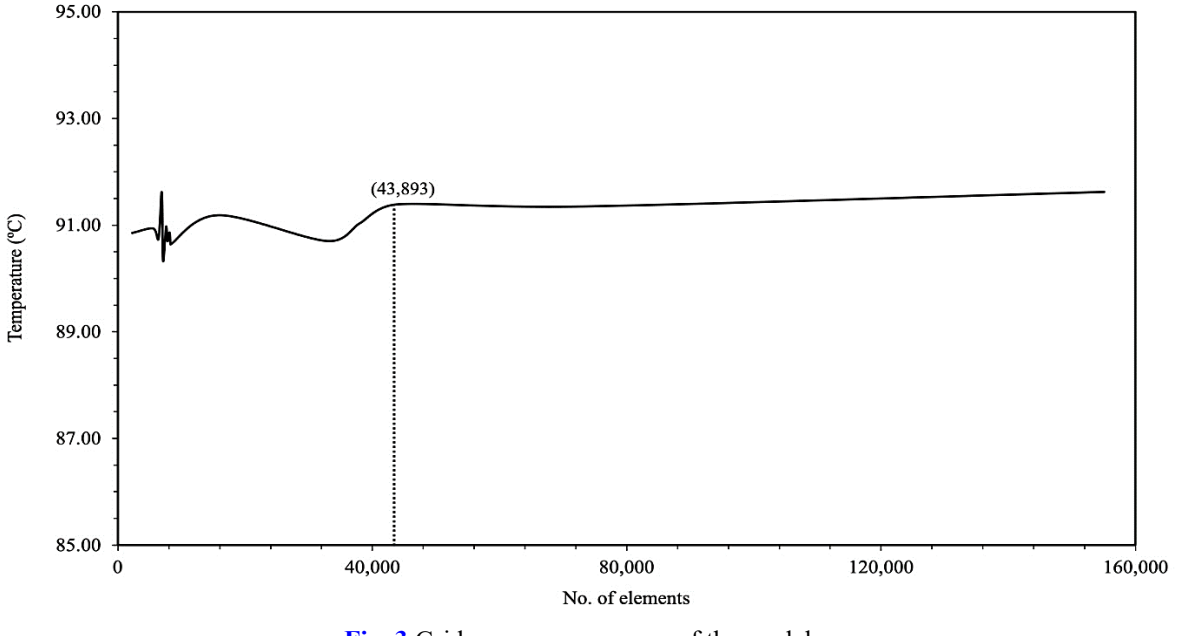

Fig. 3 Grid convergence curve of the model.

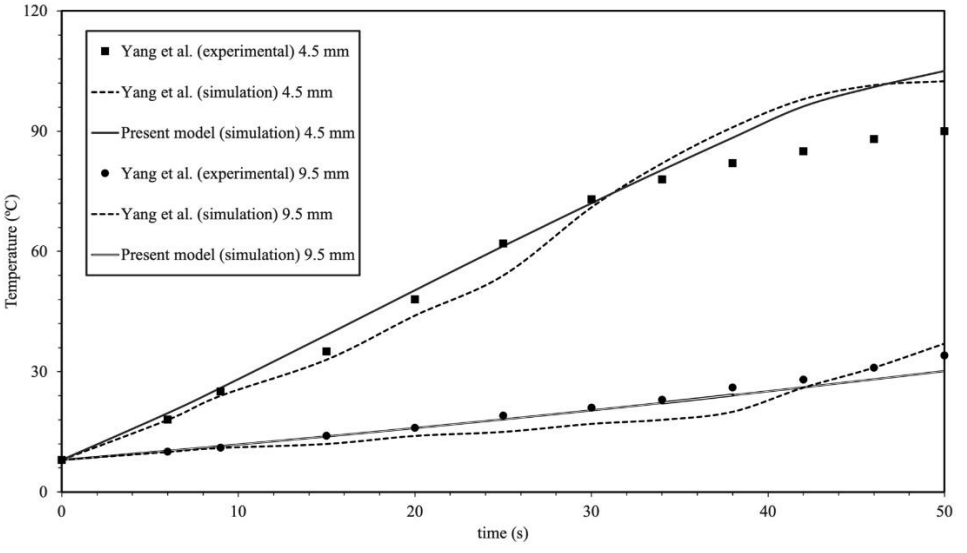

Fig. 4 The validation results of the calculated tissue temperature to the tissue temperature obtained by Yang *et al.*[15]

values between the presented simulation results and Yang *et al.*[5] compared with the experimental results obtained by Yang *et al.*[15] The verification results were clearly in good agreement with the experimental results and gave confidence in the accuracy of the presented numerical models.

Table 4. Comparisons of RMSE with results obtained by Yang *et al.*[15]

Position (mm)	Presented study	Yang *et al.* (Simulation)
4.5	7.021	7.602
9.5	1.639	3.082

5.2 Effect of property model types

This section focused on the phenomena of electromagnetic wave propagation, temperature distribution, and damage to tissue area in liver tissue during the MWA treatment process when using different property model types. The four widely property models are the constant properties model, Shao *et al.* model, Wang *et al.* model, and Xu *et al.* model. In order to the clarity demonstration effect of the property model, in all cases, the model would be applied to the same conditions such as initial condition, boundary condition, model geometry, power, microwave, microwave frequency, type of antenna slot, *etc.* Therefore, only property values are used differently for each case. The treatment time of 10 min, the microwave frequency of 2.45 GHz, and the microwave power of 45 W are used for computational. The SAR, temperature, and fraction necrotic tissue distribution in the liver tissue with different property model types during the MWA process are obtained by the numerical simulation of the electromagnetic wave propagation, heat transfer, and Arrhenius damage equations. In this study, the microwave power deposition in the liver tissue can be described by SAR distribution which leads to the analysis of temperature distribution in the liver tissue and the efficiency of the treatment process.

Figure 5 shows the 3D SAR distribution in liver tissue during the MWA treatment process of the Xu *et al.* model and captures the high-intensity SAR distribution area of the constant properties model, Wang *et al.* model, and Xu *et al.* model at the treatment time of 5 min. This result shows the SAR distribution in liver tissue, the SAR contour at the value of 1 kW/kg, and the radius size of the SAR contour for three models. Due to the Shao *et al.* model using the dielectric properties same as the constant properties model in this study, the SAR of the Shao *et al.* model shows distribution and value as same as the constant properties model. So, this section does not show the SAR distribution in the liver tissue of the Shao *et al.* model. The high-intensity SAR is distributed in the slot area and decreases with distance away from the slot, and the shape of SAR high-intensity is like a water droplet; the trend is the same for three cases. Although the trend of the SAR distribution is the same for the three cases, the result detail shows different points; the size radius SAR of 1 kW/kg and the SAR pattern by the Xu *et al.* model.

The most expansive radius size of 1 kW/kg SAR contour between Wang *et al.* and Xu *et al.* models is the same size but clearly different when compared to the constant properties model. Because of the Wang *et al.* and Xu *et al.* models are used dielectric properties with similar functions, as shown in equations 6-8. As a result, the dielectric properties of the Wang *et al.* and Xu *et al.* models are different from the constant properties model, which is constant all the treatment time. Moreover, there are some points of the SAR distribution between Wang *et al.* and Xu *et al.* models. Results from the

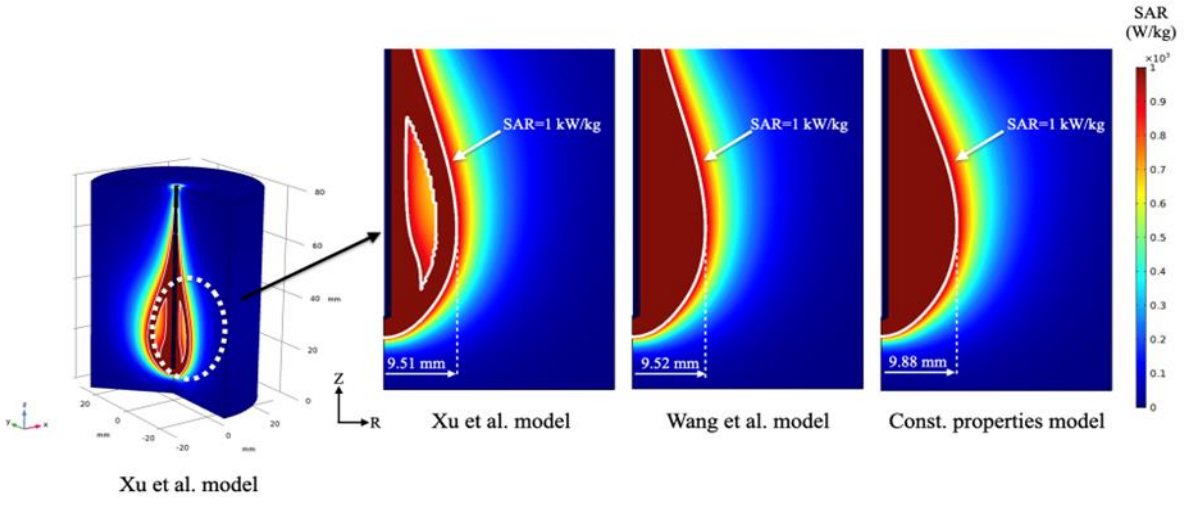

Fig. 5 3D SAR distribution in liver tissue during the MWA treatment process of the Xu *et al.* model and captures the high-intensity SAR distribution area of the constant properties model, Wang *et al.* model, and Xu *et al.* model with the microwave power of 45 W and microwave frequency of 2.45 GHz at the treatment time of 5 min.

electrical conductivity functions of the two models are different, especially in the range of the temperature is over 100 deg C. Although the 2D SAR contour and distribution in Fig. 5 could be indicated the different points when applied to the different property model types, deep detail is required for more results to clarify.

Figure 6 shows the SAR distribution in liver tissue during the MWA treatment process with the insertion depth line at the treatment time of 1 min, 5 min, and 10 min. The insertion depth line is the line parallel with the antenna and away from

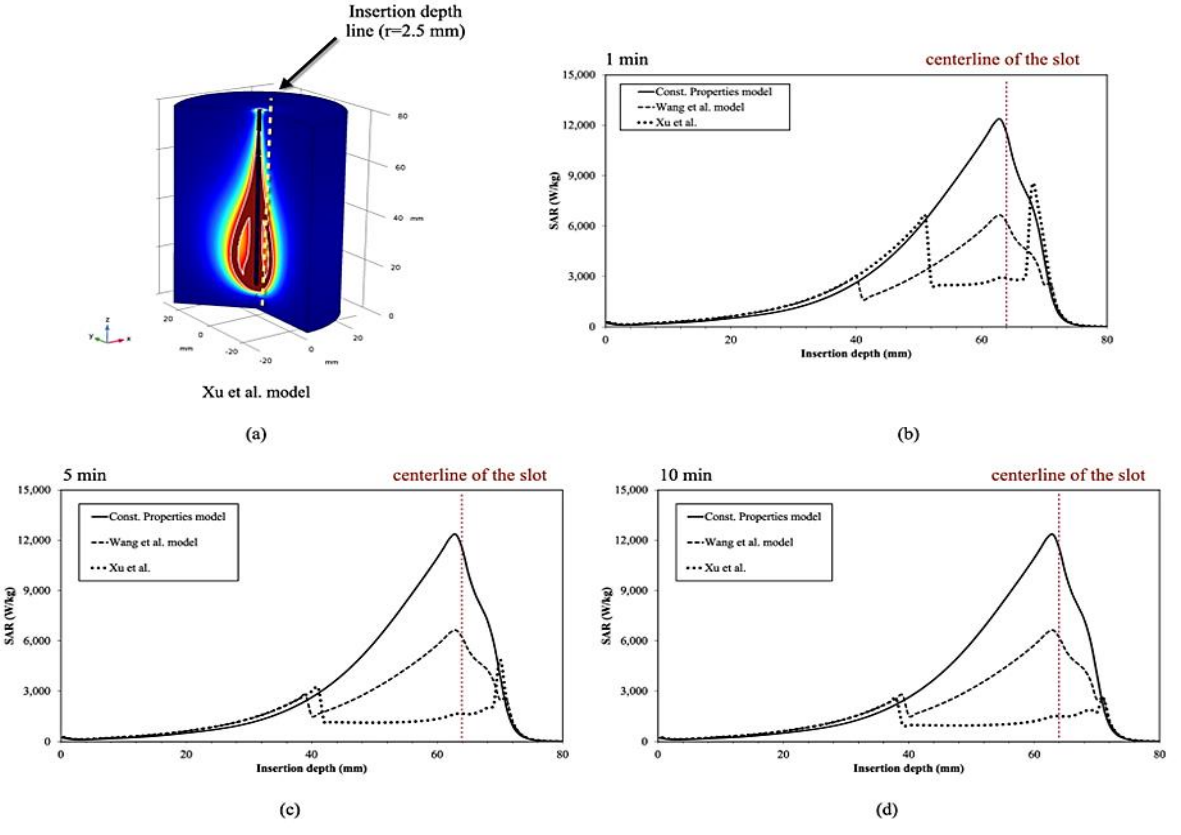

Fig. 6 SAR distribution in liver tissue during the MWA treatment process with the insertion depth line with the microwave power of 45 W and microwave frequency of 2.45 GHz; (a) 3D SAR distribution in liver tissue at the treatment time of 5 min, (b) SAR distribution with insertion depth line at the treatment time of 1 min, (c) SAR distribution with insertion depth line at the treatment time of 5 min, (d) SAR distribution with insertion depth line at the treatment time of 10 min.

the antenna centerline of 2.5 mm. In the case of the constant properties model, the maximum SAR appears around the area of the slot centerline and decreases with distance away from the slot. In this case, the SAR is not changing with the treatment time. In the case of the Wang *et al*. model, the maximum SAR appears around the area of the slot centerline, similar to the case of the constant properties model, but the magnitude is lower than the constant properties model. In addition, the SAR decreased with distance away from the slot, but at the insertion depth of 40 mm, the SAR shot up and gradually decreased again. In this case, the SAR distribution changes with treatment time, which can be observed at the insertion depth of 40 mm. In the case of the Xu *et al*. model, the SAR is a contrast distribution from any model types. The SAR shows a lower distribution in the slot area, shoots up, and gradually decreases. The shape of SAR distribution looks like a pit, and the width of the pit increases with treatment time. In this case, the SAR distribution is clearly changing with the treatment time.

Moreover, the strange contour of the Xu *et al*. model in Fig. 5 is the low SAR value, which could be caused by the temperature in this area being higher than 100 deg C. Although the SAR will be indicated the microwave energy deposit in tissue that will be converted to the external heat source generation (Q_{ext}) in liver tissue, the analysis of the SAR distribution cannot directly demonstrate the heat transfer phenomenon in liver tissue during the MWA treatment process. Thus, the temperature distribution is needed to demonstrate.

Figure 7 shows the temperature contour and distribution in liver tissue during the MWA treatment process of the constant properties model, Shao *et al*. model, Wang *et al*. model, and Xu *et al*. model at the treatment time of 5 min. The shape of the hot spot zone of the four models is quietly different. The radius of the 60 deg C temperature line of the constant properties model, Shao *et al*. model, Wang *et al*. model, and Xu *et al*. model is 15.11 mm, 17.39 mm, 11.46 mm, and 13.52 mm, respectively. The height of the 60 deg C temperature line of the constant properties model, Shao *et al*. model, Wang *et al*. model, and Xu *et al*. model is 50.20 mm, 53.44 mm, 53.39 mm, and 45.95 mm, respectively. The hot spot zone from the Shao *et al*. model is more comprehensive than other models, and the hot spot zone from the Wang *et al*. model is smaller than other models. The hot spot shape of the constant properties model, Shao *et al*. model, and Wang *et al*. model could be observed in the hot spot tail over the slot area, while the hot spot shape of the Xu *et al*. model could not be observed in the hot spot tail. In addition, the hot spot size of the Wang *et al*. model is quite different from the other models.

Figure 8 shows the temperature distribution in liver tissue during the MWA treatment process with the insertion depth line at the treatment time of 1 min, 5 min, and 10 min. The insertion depth line is the line parallel with the antenna and away from the antenna centerline of 2.5 mm. The temperature peaks around the slot area and decreases with distance away from the slot. Although the temperature peaks and decreases in a similar position, the model's temperature distribution pattern and magnitude are different. For the treatment time of 1 min, The temperature distribution of constant properties, Shao *et al*., and Wang *et al*. models are similar patterns, as shown in Fig. 8(b). The temperature distribution of the Wang

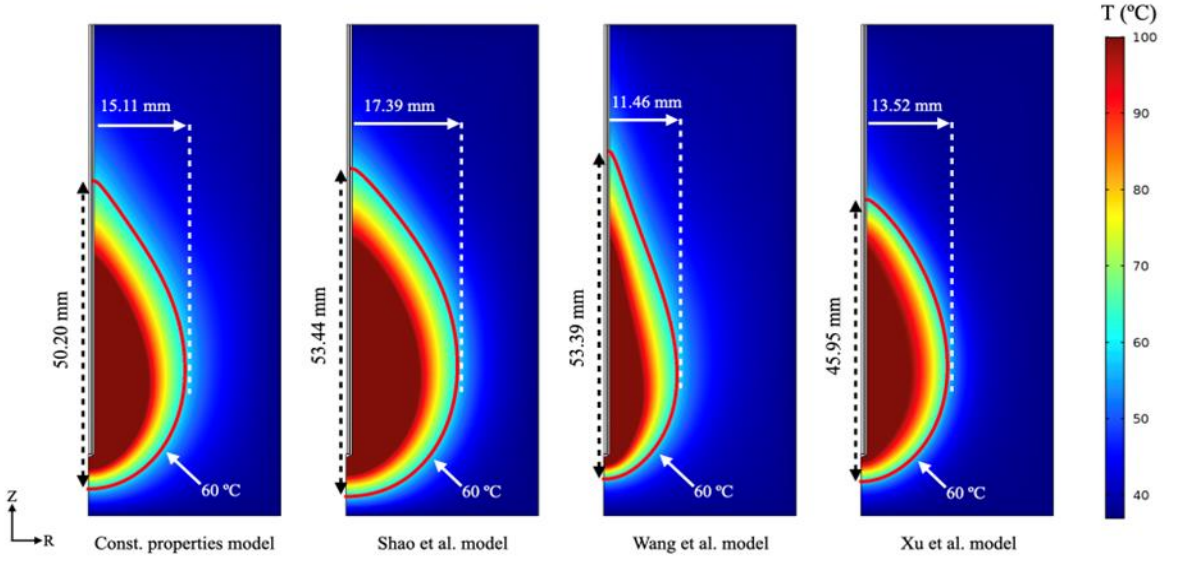

Fig. 7 The temperature contour and distribution in liver tissue during the MWA treatment process of the constant properties model, Shao *et al.* model, Wang *et al.* model, and Xu *et al.* model with the microwave power of 45 W and microwave frequency of 2.45 GHz at the treatment time of 5 min.

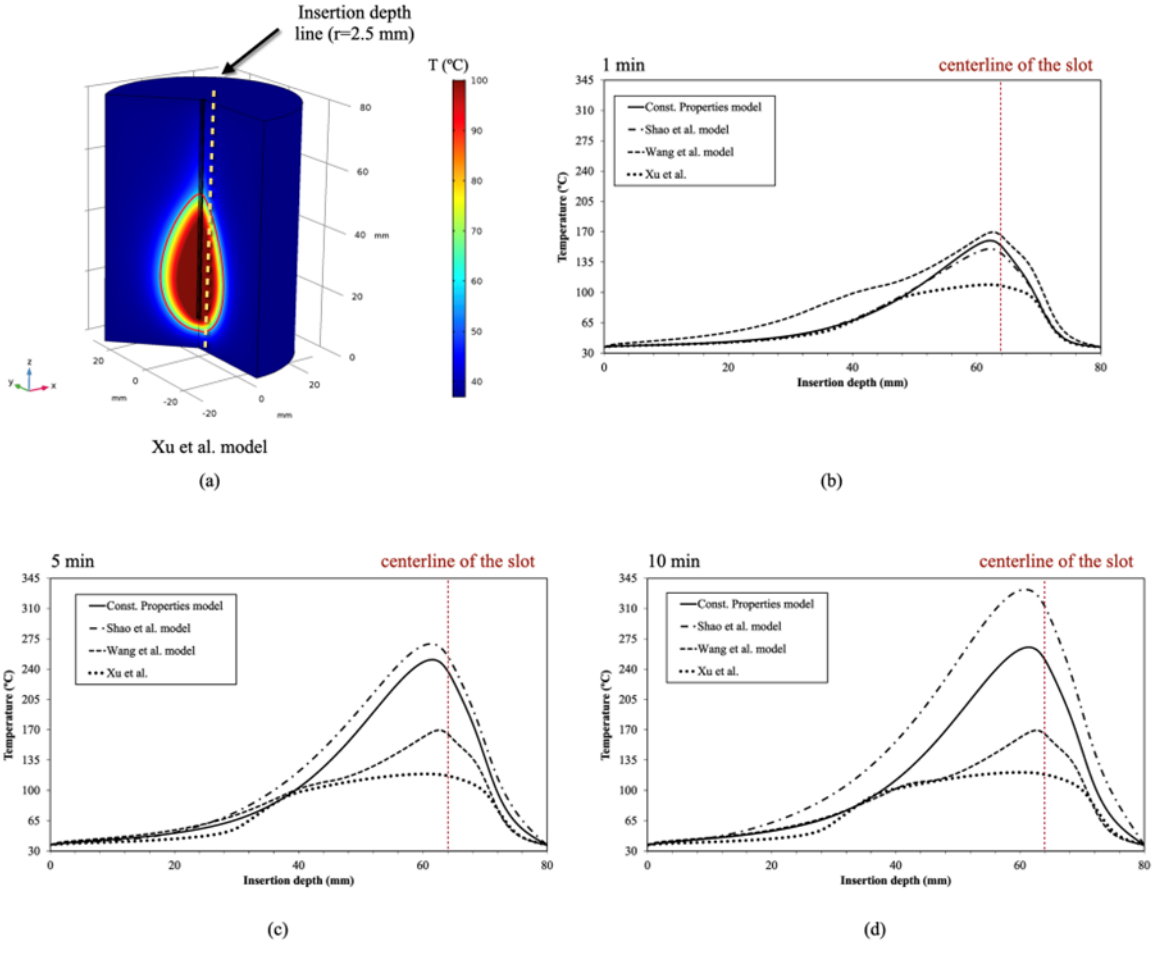

Fig. 8 The temperature distribution in liver tissue during the MWA treatment process with the insertion depth line with the microwave power of 45 W and microwave frequency of 2.45 GHz; (a) 3D temperature distribution in liver tissue by using Xu *et al.* model at the treatment time of 5 min, (b) Temperature distribution with insertion depth line at the treatment time of 1 min, (c) Temperature distribution with insertion depth line at the treatment time of 5 min, (d) Temperature distribution with insertion depth line at the treatment time of 10 min.

et al. model is highest and followed by the constant properties model, Shao *et al*. model, and Xu *et al*. model, respectively. The temperature distribution of the Xu *et al*. model is the lowest and quite different from other models. However, in this case, the temperature distribution of the Xu *et al*. model corresponds with the SAR of the Xu *et al*. model. In the point of interest, the SAR distribution by Wang *et al*. model is lower than the constant properties model, but the temperature distribution by Wang *et al*. model is higher than the constant properties model. Thus, specific thermal properties may result in this phenomenon, but these results cannot indicate the high impact properties.

For the treatment time of 5 and 10 min, the temperature distribution of the Shao *et al*. model is the highest and followed by the constant properties model, Wang *et al*. model, and Xu *et al*. model, respectively. These temperature results correspond with the SAR distribution in the previous section. The temperature distribution by the constant properties model and Shao *et al*. model is increased with the treatment time, and it is clearly observed by the overall distribution and maximum temperature. The temperature distribution by Wang *et al*. model is slightly different with treatment time increasing. The temperature distribution by Xu *et al*. model is different with treatment time increasing, but it is a different pattern from other models. In the other model, the highest temperature point will be increased at the slot area and decrease with the distance away from the slot. However, in the temperature distribution of the Xu *et al*. model, the highest temperature is almost unchanged with increasing treatment time. But the high temperature will be expanded before gradually decreasing according to the distance away from the slot because the Xu *et al*. model is developed under the assumption that the electrical conductivity of tissue is lower than the other models at the high temperature. The temperature distribution difference

between the property models will occur when the tissue temperature is higher than 100 deg C, which models are used different property values. The temperature difference could be clearly observed in the slot area, which is the hot spot area. Moreover, the temperature difference between the property models has increased with the treatment time.

Furthermore, this study demonstrated the fraction of necrotic tissue (θ_d) that indicates the performance of the MWA treatment process. The fraction of necrotic tissue evaluates the damage in liver tissue during the treatment process. When tissues get more energy, that means the heat from the treatment process. The damage increases with the amount of heat interaction in the tissue, as shown in equation 25. The fraction of necrotic tissue is the level of tissue damage, $\theta_d = 0$ indicates no damage in the liver tissue. In contrast, $\theta_d = 1$ indicates a fully damaged liver tissue. Fig. 9 shows the fraction of necrotic tissue during the MWA treatment process of the constant properties model, Shao *et al*. model, Wang *et al*. model, and Xu *et al*. model at the treatment time of 10 min. The fully damaged area of the constant properties model, Shao *et al*. model, Wang *et al*. model, and Xu *et al*. model is 854.8 mm^2, 1,104.9 mm^2, 627.3 mm^2, 527.4 mm^2, respectively. In this study, the area liver tissue domain is 2,337.1 mm^2. The fully damaged area of the Shao *et al*. model is the largest, followed by the constant properties model, Wang *et al*. model, and Xu *et al*. model. The fraction of necrotic tissue distribution corresponds with SAR and temperature distribution. Fig. 10 shows the fully damaged area in the liver tissue during the MWA treatment process when using different property models. For all cases, the fully damaged area increases with the treatment time, the area by the Shao *et al*. model is highest, followed by the constant properties model, Wang *et al*. model, and Xu *et al*. model. In the initial stage of treatment, the fully damaged area of the constant properties model, Shao *et al*. model, and Xu *et al*. models are increased with a similar trend. After that, the fully damaged area of the Xu *et al*. model increases with a lower slope, which likes as a result of the Wang *et al*. model. The result of the constant properties and Shao *et al*. models is increased with the same trend, but the Shao *et al*. model is higher increasing than the constant properties model. This result demonstrates the effect of the model that considered the dielectric properties function with the temperature, and the model is considered constant dielectric properties.

Although the property models are used to predict the SAR and temperature distribution in the liver during the MWA treatment process with the same condition and the same situation, the result of the models demonstrated the difference in SAR distribution, temperature distribution, and damaged tissue area. Significantly, the models have considered dielectric properties depending on the temperature, and models have considered constant value. Although Wang *et al*. model and Xu *et al*. model seem to be able to predict the phenomenon at hot spot areas better than the other models, this result is not a conclusion that causes from what properties.

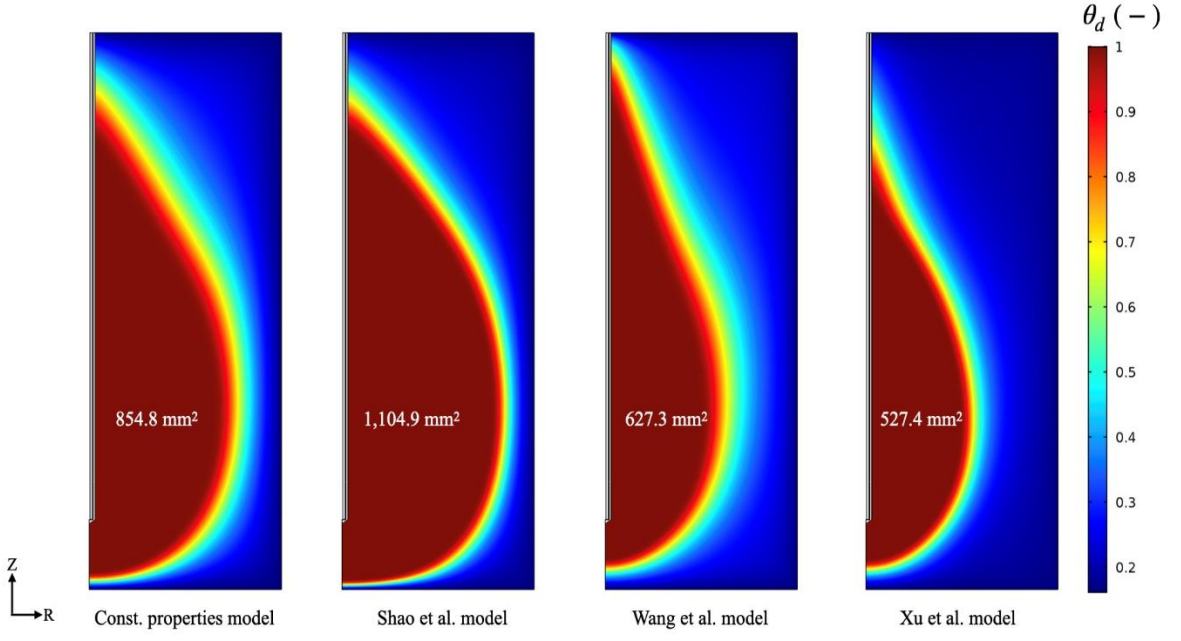

Fig. 9 The fraction of necrotic tissue distribution and damaged area in the liver tissue during the MWA treatment process of the constant properties model, Shao *et al.* model, Wang *et al.* model, and Xu *et al.* model with the microwave power of 45 W and microwave frequency of 2.45 GHz at the treatment time of 5 min.

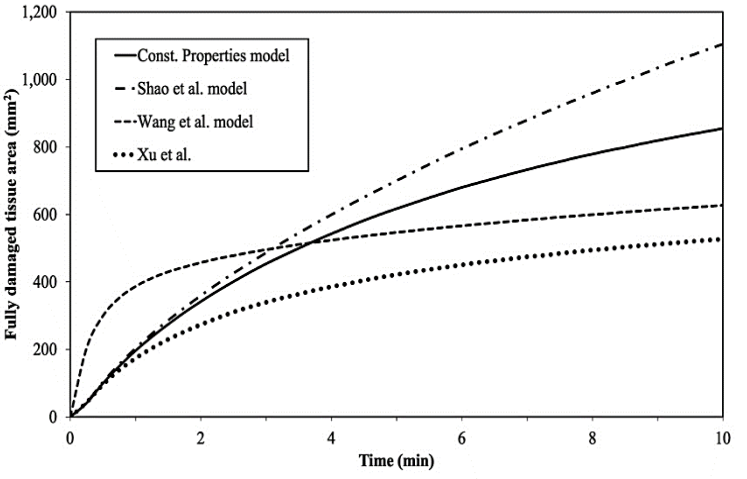

Fig. 10 The transient fully damaged area in the liver tissue during the MWA treatment process when using different properties model types.

Therefore, the next section will be demonstrated each of the property functions that affect the thermal response in the liver tissue during the MWA process.

5.4 Influence of the property function characteristics

This section focused on the effect of each property function on the thermal response in the liver tissue during the MWA treatment process with a microwave frequency of 2.45 GHz and power of 45 W for all cases. The properties functions are investigated by applying each property function in the constant properties model, one by one function, i.e., when investigating the electrical conductivity function, the relative permittivity, blood perfusion rate, thermal conductivity, and specific heat capacity are considered with a constant. All the property functions to be investigated are relative permittivity by Wang *et al*., electrical conductivity by Wang *et al*., electrical conductivity by Xu *et al*., blood perfusion rate by Shao *et al*., blood perfusion rate by Wang *et al*., blood perfusion rate by Xu *et al*., thermal conductivity by Shao *et al*., thermal conductivity by Wang *et al*., thermal conductivity by Xu *et al*., specific heat capacity by Wang *et al*., and specific heat capacity by Xu *et al*. The thermal response in the liver tissue represented on the temperature distribution that is obtained by the numerical simulation of the electromagnetic wave propagation, heat transfer, and Arrhenius damage equations.

Figure 11 shows the temperature contour and distribution in liver tissue during the MWA treatment process of the constant properties model, the relative permittivity by Wang *et al*., the electrical conductivity by Wang *et al*., and the electrical conductivity by Xu *et al*. at the treatment time of 5 min. The dimension of the 60 deg C temperature contour shows in this figure. The area of tissue temperature is higher than 60 deg C of the constant properties model, the relative permittivity by

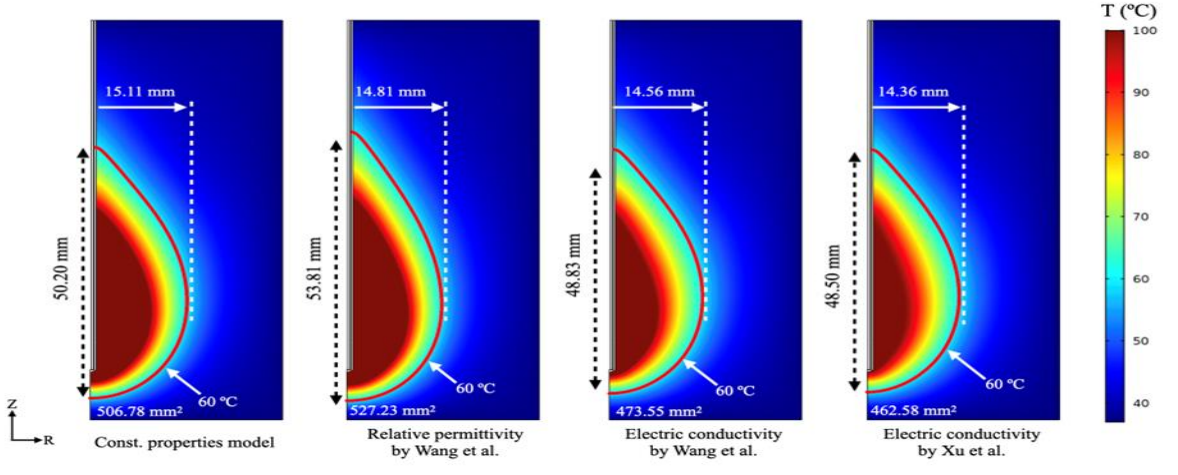

Fig. 11 The temperature contour and distribution in liver tissue during the MWA treatment process with the microwave power of 45 W and microwave frequency of 2.45 GHz of the constant properties model, the relative permittivity by Wang et al., the electrical conductivity by Wang et al., and the electrical conductivity by Xu et al. at the treatment time of 5 min.

Wang *et al*., the electrical conductivity by Wang *et al*., and the electrical conductivity by Xu *et al*. are 506.78 mm^2, 527.23 mm^2, 473.55 mm^2, and 462.58 mm^2, respectively. The model has applied a relative permittivity function that shows the hot spot area is higher than the constant model. In contrast, the models have applied the electrical conductivity function that shows the hot spot area is lower than the constant model. The SAR and temperature distribution with the insertion depth line show the results from the model with the relative permittivity by Wang *et al*. that is higher than the other models, as shown in Fig. 12(a) and Fig. 12(b). In the models that have applied the electrical conductivity function, the SAR and temperature distribution with the insertion depth line are lower than in the other models. These results demonstrated the effect of the electrical conductivity function higher than the relative permittivity function, especially the electrical conductivity by Xu *et al*.

Figure 12(c) shows that the relative permittivity between the constant value and Wang *et al*. depends on the tissue temperature. In the case of the relative permittivity by Wang *et al*., the relative permittivity will be started at 34.01 and gradually decreases with the temperature increases, as shown in equation 6. The relative permittivity will be dropped to 16.67 and constant in this value at tissue temperature over 100 deg C. And Fig. 12(d) shows that the electrical conductivity between the constant value, Wang *et al*., and Xu *et al*. depends on the tissue temperature. Similar to the relative permittivity function, the electrical conductivity will drop to a low value when the tissue temperature is over 100 deg C. The relative permittivity by Xu *et al*. is the lowest in the high temperature, followed by the Wang *et al*. and constant value, respectively. The relative permittivity represents the ability of the insulator to store electric energy when exposed to the electrical field in the material. The relative permittivity is a low value, the energy from the electrical field is permitted difficultly in the material compared with the high relative permittivity. In this case, the electrical field of the low relative permittivity will be generated with the same quality and low propagation. As a result, the heat generated by the electric field is higher the other cases but with a low distribution. The electrical conductivity represents the ability to conduct the electric current of the material, which affects the SAR distribution and

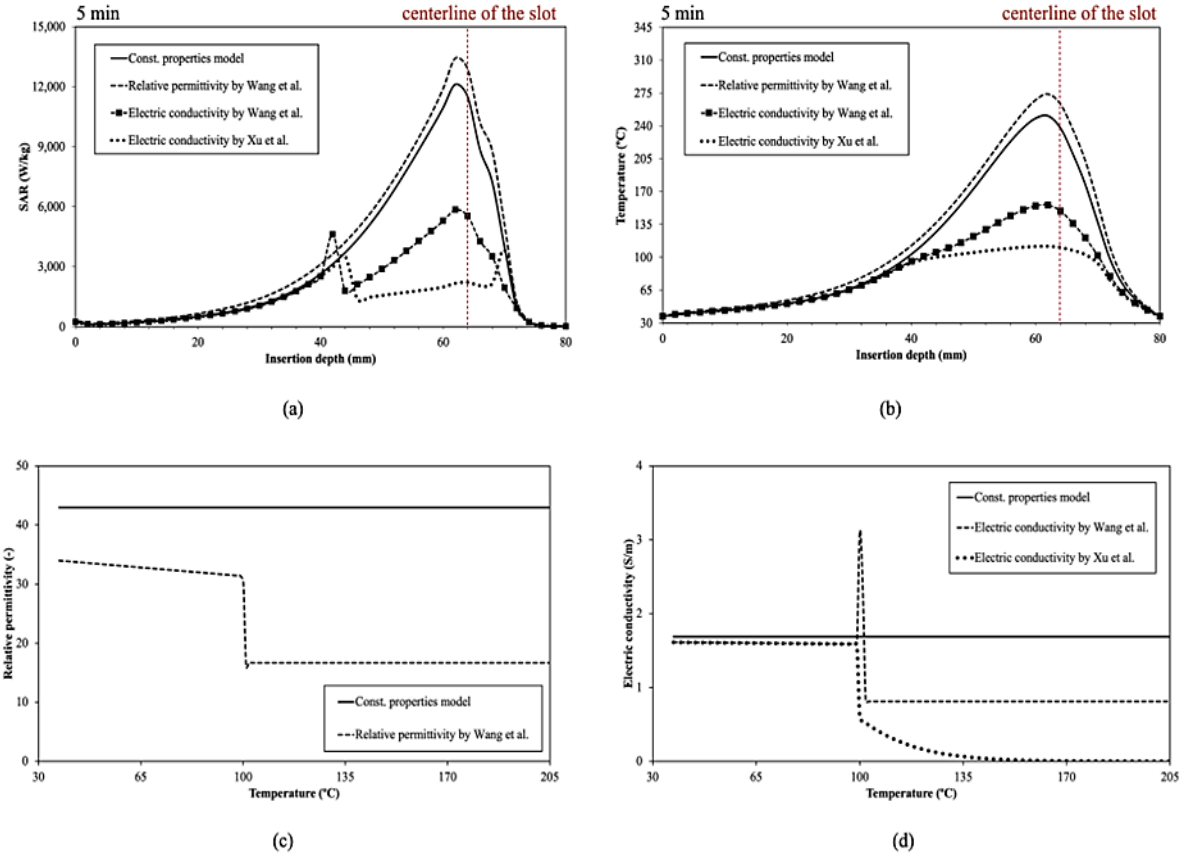

Fig. 12 The SAR and temperature distribution along with the insertion depth line and property functions depending on the tissue temperature of the constant properties model, the relative permittivity by Wang *et al.*, the electrical conductivity by Wang *et al.*, and the electrical conductivity by Xu *et al.*; (a) SAR distribution along with the insertion depth line, (b) Temperature distribution along with the insertion depth line; (c) The relative permittivity functions depend on the tissue temperature, (d) The electrical conductivity functions depend on the tissue temperature.

external heat generation, as shown in equations 4-5. The relative permittivity and electrical conductivity of tissue depend on tissue temperature and affect predicting the thermal response in the liver tissue during the MWA treatment process, significantly if the tissue temperature is exceeded 100 deg C. Although the relative permittivity and electrical conductivity of tissue are related, the result demonstrated the effect of the electrical conductivity function higher than the relative permittivity function during the MWA process.

Fig. 13 shows the temperature contour and distribution in liver tissue during the MWA treatment process of the constant properties model, the blood perfusion rate by Shao *et al*., the blood perfusion rate by Wang *et al*., and the blood perfusion rate by Xu *et al*. at the treatment time of 5 min. The dimension of the 60 deg C temperature contour shows in this figure. The area of tissue temperature is higher than 60 deg C of the constant properties model, the blood perfusion rate by Shao *et al*., the blood perfusion rate by Wang *et al*., and the blood perfusion rate by Xu *et al*. at the treatment time of 5 min are 506.78 mm2, 633.04 mm2, 357.35 mm2, and 440.11 mm2, respectively. The hot spot area of the blood perfusion rate by Shao *et al*. is more extensive than in other blood perfusion rate models, and the hot spot area of the blood perfusion rate by Wang *et al*. is lower than in other blood perfusion rate models. Fig. 14 shows the temperature contour and distribution in liver tissue during the MWA treatment process of the constant properties model, the thermal conductivity by Shao *et al*., the thermal conductivity by Wang *et al*., and the thermal conductivity by Xu *et al*. at the treatment time of 5 min. The dimension of the 60 deg C temperature contour shows in this

Table 5. The Ablation area of parameters considered in this study.

Properties model	The Ablation area (T > 60ºC)	The difference hot spot area when compared with the constant properties
Const. properties model	506.78 mm^2	0 mm^2
Relative permittivity by Wang *et al*.	527.23 mm^2	20.45 mm^2 (4.04%)
Electric conductivity by Wang *et al*.	473.55 mm^2	33.23 mm^2 (6.56%)
Electric conductivity by Xu *et al*.	462.58 mm^2	44.2 mm^2 (8.72%)
Blood perfusion rate by Shao *et al*.	633.04 mm^2	126.26 mm^2 (24.91%)
Blood perfusion rate by Wang *et al*.	357.35 mm^2	149.43 mm^2 (29.49%)
Blood perfusion rate by Xu *et al*.	440.11 mm^2	66.67 mm^2 (13.16%)
Thermal conductivity by Shao *et al*.	514.16 mm^2	7.38 mm^2 (1.46%)
Thermal conductivity by Wang *et al*.	484.69 mm^2	22.09 mm^2 (4.36%)
Thermal conductivity by Xu *et al*.	513.54 mm^2	6.76 mm^2 (1.33%)
Specific heat capacity by Shao *et al*.	504.71 mm^2	2.07 mm^2 (0.41%)
Specific heat capacity by Wang *et al*.	623.97 mm^2	117.19 mm^2 (23.12%)

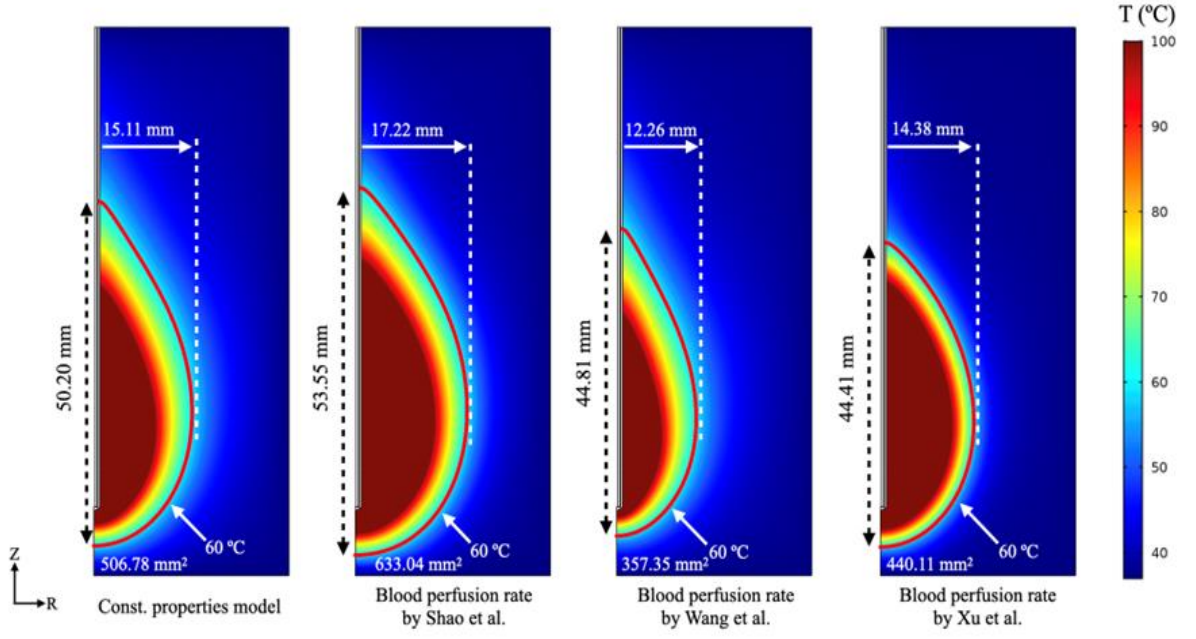

Fig. 13 The temperature contour and distribution in liver tissue during the MWA treatment process with the microwave power of 45 W and microwave frequency of 2.45 GHz of the constant properties model, the blood perfusion rate by Shao *et al*., the blood perfusion rate by Wang *et al*., and the blood perfusion rate by Xu *et al*. at the treatment time of 5 min.

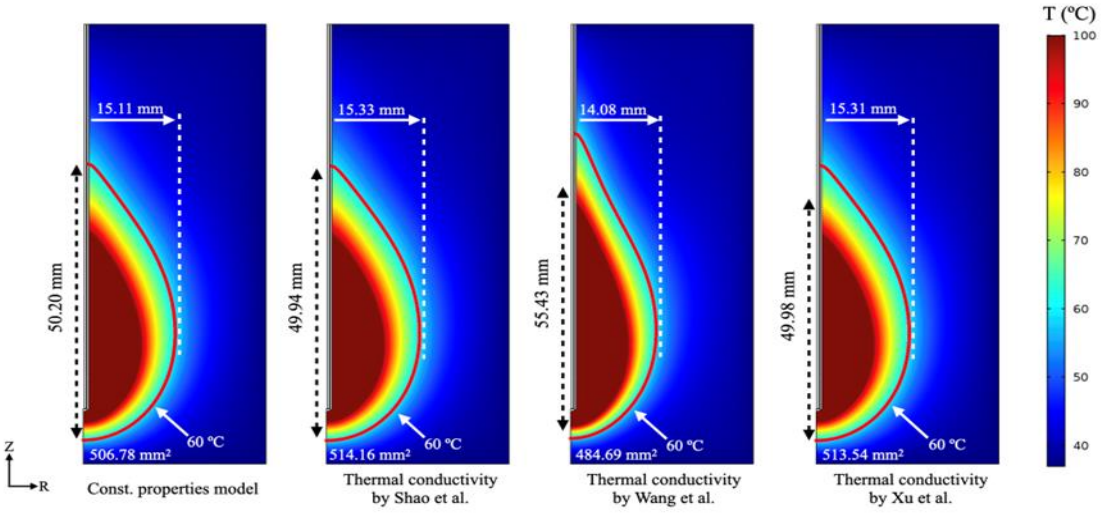

Fig. 14 The temperature contour and distribution in liver tissue during the MWA treatment process with the microwave power of 45 W and microwave frequency of 2.45 GHz of the constant properties model, the thermal conductivity by Shao *et al.*, the thermal conductivity by Wang *et al.*, and the thermal conductivity by Xu *et al.* at the treatment time of 5 min.

figure. The area of tissue temperature is higher than 60 deg C of the constant properties model, the thermal conductivity by Shao *et al*., the thermal conductivity by Wang *et al*., and the thermal conductivity by Xu *et al*. at the treatment time of 5 min are 506.78 mm2, 514.16 mm2, 484.69 mm2, and 513.54 mm2, respectively. In this case, the hot spot area of the models is a similar size, except that the hot spot area of the thermal conductivity by Wang *et al*. is lower than in other thermal conductivity models. Fig. 15 shows the temperature contour and distribution in liver tissue during the MWA treatment process of the constant properties model, the specific heat capacity by Shao *et al*., and the specific heat capacity by Wang *et al*. at the treatment time of 5 min. The dimension of the 60 deg C temperature contour shows in this figure. The area of tissue temperature is higher than 60 deg C of the constant properties model, the specific heat capacity by Shao *et al*., and the specific heat capacity by Wang *et al*. at the treatment time of 5 min are 506.78 mm2, 504.71 mm2, and 623.97 mm2, respectively. This case shows that the hot spot area of the specific heat capacity by Wang *et al*. is more expansive than in other specific heat capacity models.

Figure 16 shows the comparison temperature distribution with the insertion depth line between the blood perfusion rate models, thermal conductivity models, and the specific heat capacity models at the treatment time of 5 min. All cases show the high temperature around the slot area and decrease with the distance away from the slot. In the blood perfusion rate functions, the temperature distribution of the blood perfusion

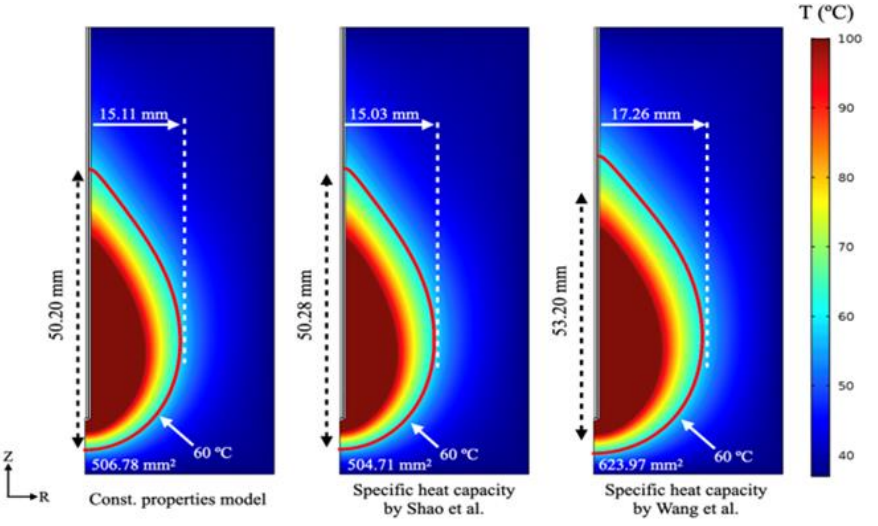

Fig. 15 The temperature contour and distribution in liver tissue during the MWA treatment process with the microwave power of 45 W and microwave frequency of 2.45 GHz of the constant properties model, the specific heat capacity by Shao *et al*., and the specific heat capacity by Wang *et al*. at the treatment time of 5 min.

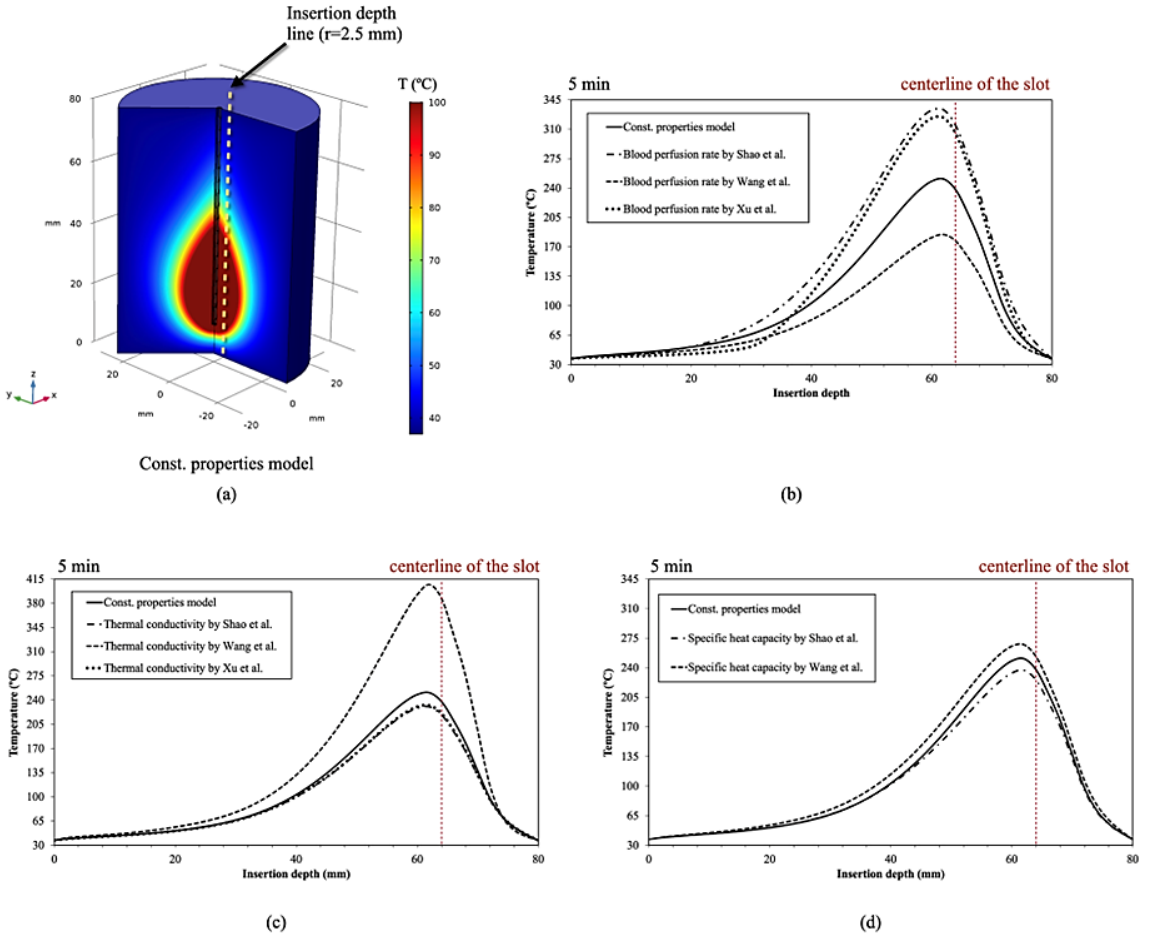

Fig. 16 The temperature distribution in liver tissue during the MWA treatment process with the insertion depth line with the microwave power of 45 W and microwave frequency of 2.45 GHz at the treatment time of 5 min; (a) 3D temperature distribution in liver tissue by using constant properties model, (b) The comparison temperature distribution between blood perfusion rate functions, (c) The comparison temperature distribution between thermal conductivity functions, (d) The comparison temperature distribution between specific heat capacity functions.

rate by Shao *et al*. is the highest increase, followed by the Xu functions, the temperature distribution of thermal conductivity by Wang *et al*. is the highest and different from the other thermal conductivity models, as shown in Fig. 16(c). In the specific heat capacity function, the temperature distribution of the specific heat capacity Wang *et al*. is slightly higher than the constant properties model and the specific heat capacity by Shao *et al*., respectively.

Figure 17 shows the blood perfusion rate functions, thermal conductivity functions, remaining water content in tissue, and specific heat capacity functions depending on the tissue temperature. In Fig. 17(a), the blood perfusion rate of the constant properties is 0.0036 1/s and constant in all of the temperatures. The blood perfusion rate of Wang *et al*. is increased with temperature, and the blood perfusion rate of Xu *et al*. is stated at 0.016 1/s and dropped to 0 1/s when the tissue temperature exceeded 60 deg C. In the blood perfusion rate by Shao *et al*., the function is dependent on the degree of tissue injury (Ω), in which the degree of tissue injury depends upon the tissue temperature. It is quite difficult to directly explain the relationship between blood perfusion rate and tissue temperature. Thus, it is not shown in this figure. However, in Fig. 16(b), the temperature distribution of the blood perfusion rate by Shao *et al*. and Xu *et al*. represent a similar result because these two functions are developed under a similar concept that the blood perfusion rate is dropped to zero when tissue is dead, and the high temperature is the cause of the tissue dead. On the other side, the blood perfusion rate by Wang *et al*. referred to Keangin *et al*. study that developed the MWA treatment in the liver tissue under the tissue temperature is not exceeded 100 deg C. Therefore, the blood perfusion rate by Shao *et al*. and Xu *et al*. concepts is more advantage than the other models.

In Fig. 17(b), the thermal conductivity of the constant properties model is 0.497 W/m.K and constant in all of the temperatures. The thermal conductivity of Shao *et al*. and Xu

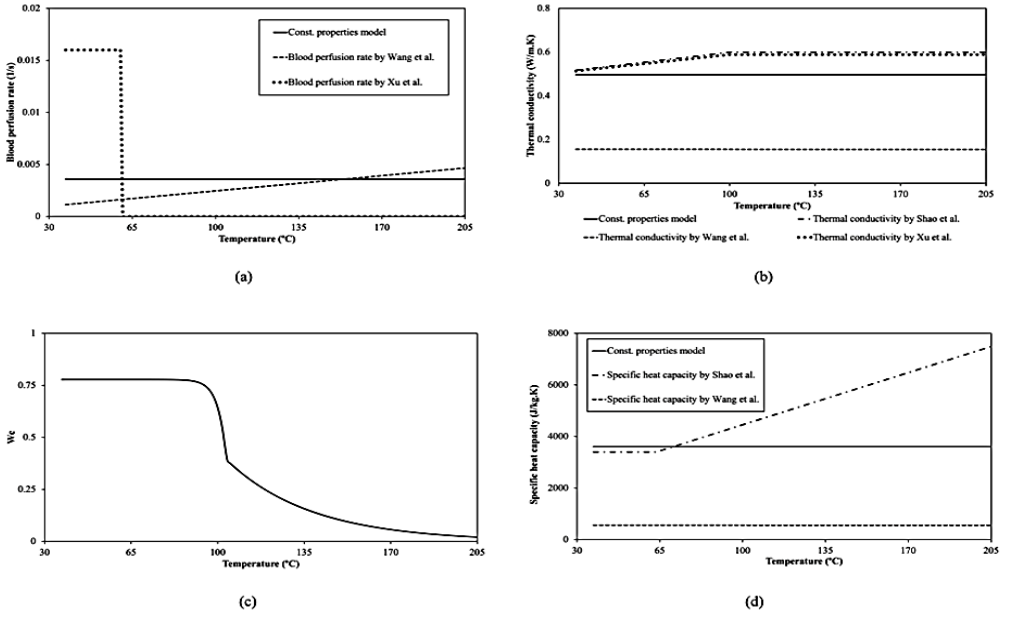

Fig. 17 The blood perfusion rate functions, thermal conductivity functions, remaining water content in tissue, and specific heat capacity functions depending on the tissue temperature; (a) Blood perfusion rate functions, (b) Thermal conductivity functions, (c) the remaining water content in the tissue during the ablation process, (d) Specific heat capacity functions.

et al. increases with temperature. These two functions are developed under a similar concept that the thermal conductivity will be increased with the tissue temperature. Because the tissue structure will be changed when the tissue temperature is higher, but tissue temperature is over some point, the tissue structure will not change at that point is 100 deg C. Thus, the thermal conductivity of Shao *et al*. and Xu *et al*. will be increased during the tissue temperature under of 100 deg C, and it will be constant when the tissue temperature exceeded that point. In the thermal conductivity by Wang *et al*., this function is developed under tissue evaporation during the MWA treatment process. This function calculates the remaining water content in the tissue during the process, as shown in Fig. 17(c). This concept is proposed by Yang *et al*. study, the water content in the liver tissue had remained around 0.778 and decreased when the tissue temperature increased. Although the thermal conductivity by Wang *et al*. is a good concept, the value function is quite different from the other functions and the thermal conductivity value by previous literature.[16,20,29] However, the thermal conductivity function slightly affects the temperature prediction, as shown in Fig. 16(c), except for the thermal conductivity by Wang *et al*. In Fig. 17(d), the specific heat capacity by the constant properties model is 3,600 J/kg.K and constant in all of the temperatures. The specific heat capacity by Shao *et al*. is stable in the initial temperature and gradually increases when the tissue temperature increases. On the other side, the specific heat capacity by Wang *et al*. is a little bit changing when the tissue temperature increases. Although the specific heat capacity between the three models is different, the temperature distribution is slightly different.

Figure 18 shows the temperature distribution with an insertion depth line between relative permittivity by Wang *et al*., electrical conductivity by Xu *et al*., blood perfusion rate by Xu *et al*., thermal conductivity by Shao *et al*., thermal conductivity by Wang *et al*., and specific heat capacity by Wang *et al*. at the treatment time of 5 min. These functional properties affect the distribution of high tissue temperature compared to the constant properties model. The function that affects the tissue temperature distribution the most is the electrical conductivity by Xu *et al*., followed by thermal conductivity by Wang *et al*., blood perfusion rate by Shao *et al*., relative permittivity by Wang *et al*., thermal conductivity by Shao *et al*., and specific heat capacity by Wang *et al*., respectively. However, the thermal conductivity by Wang et al. is not corresponding with the previous study and is more different from other thermal conductivity functions, as shown in Fig. 17(b). Thus, this study will suggest the thermal conductivity of Shao *et al*. than Wang *et al*.

This section proposed the influence of each property characteristic on the temperature distribution in liver tissue during the MWA treatment process. The results show the difference in the tissue temperature distribution when using a different function even if the same type of the properties. The most property functions affecting tissue temperature prediction is electrical conductivity, followed by blood

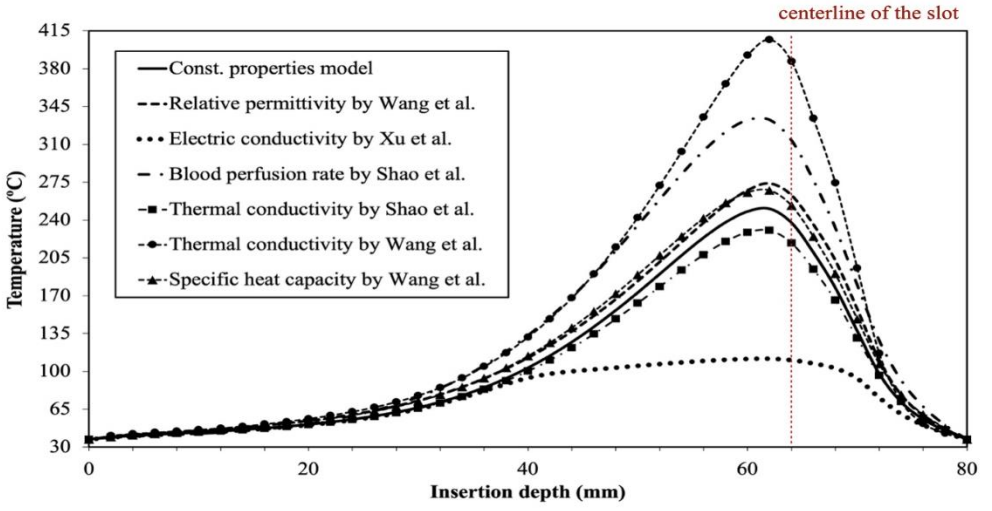

Fig. 18 The temperature distribution with an insertion depth line between relative permittivity by Wang *et al*., electrical conductivity by Xu *et al*., blood perfusion rate by Xu *et al*., thermal conductivity by Shao *et al.*, thermal conductivity by Wang *et al.*, and specific heat capacity by Wang *et al.* with the microwave power of 45 W and microwave frequency of 2.45 GHz at the treatment time of 5 min.

perfusion rate, relative permittivity, thermal conductivity, and specific heat capacity, respectively. The main reason for the difference is that some functions consider the effect of evaporation during the ablation process, but some properties are not considered. However, some properties functions induced the tissue temperature to be higher than the properties constant model, but some properties functions reduced the tissue temperature lower than the properties constant model. The next section will propose the comparison suggestion properties model with the constants properties model to demonstrate the effects of all property functions in the actual model.

In some studies, some group research can be avoided this limitation by considering the MWA process with low microwave power, such as the studies by Keangin *et al*. However, this limitation cannot be avoided forever.

5.4 The comparison suggestion properties model with constants properties model

This section demonstrates the thermal response in the liver tissue during the MWA treatment process with a microwave frequency of 2.45 GHz and power of 45 W between the suggestion properties model and the constants properties model. The suggestion model consists of the electrical conductivity by Xu *et al*., blood perfusion rate by Shao *et al*., relative permittivity by Wang *et al*., thermal conductivity by Shao *et al*., and specific heat capacity by a constant value, which is suggested in previous sections. The specific heat capacity function is considered with a constant value because the specific heat capacity function slightly affects the tissue temperature distribution. Thus, this suggestion is used a specific heat capacity of liver tissue with a constant value.

Figure 19 shows the SAR and temperature distribution in the liver tissue during the MWA treatment process with a microwave frequency of 2.45 GHz and power of 45 W between the suggestion properties model and the constants properties model at the treatment time of 5 min. The dimensions of the hot spot area between the suggestion properties model and the constant properties model as shown in Figs. 19(b) and 19(c). The hot spot of the suggestion properties model is large than the hot spot of the constant properties model. The SAR distribution in the insertion depth line (r=2.5 mm) of the suggestion properties model is lower than the constant properties model, as shown in Fig. 19(d). And the temperature distribution in the insertion depth line (r=2.5 mm) of the suggestion properties model is lower than the constant properties model according to the SAR distribution, as shown in Figs. 19(d)-19(e).

Figure 19 The SAR and temperature distribution in the liver tissue during the MWA treatment process with a microwave frequency of 2.45 GHz and power of 45 W between the suggestion properties model and the constants properties model with the microwave power of 45 W and microwave frequency of 2.45 GHz at the treatment time of 5 min; (a) 3D temperature distribution in liver tissue by using the suggestion model, (b) The temperature contour and distribution of the constant properties model, (c) The temperature contour and distribution of the suggestion model, (d) The comparison SAR distribution along with the insertion depth line of the constant properties model and suggestion

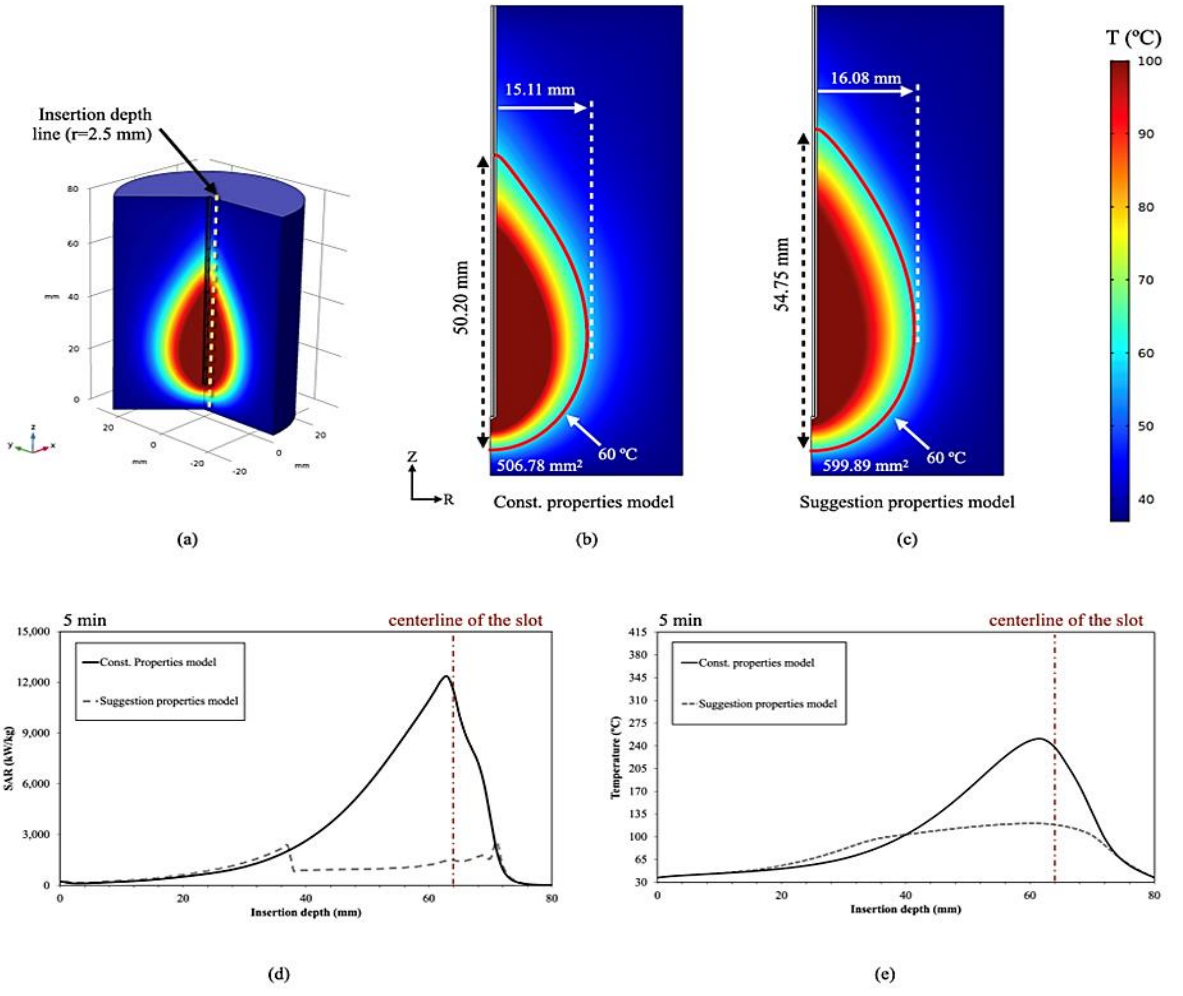

Fig. 19 The SAR and temperature distribution in the liver tissue during the MWA treatment process with a microwave frequency of 2.45 GHz and power of 45 W between the suggestion properties model and the constants properties model with the microwave power of 45 W and microwave frequency of 2.45 GHz at the treatment time of 5 min; (a) 3D temperature distribution in liver tissue by using the suggestion model, (b) The temperature contour and distribution of the constant properties model, (c) The temperature contour and distribution of the suggestion model, (d) The comparison SAR distribution along with the insertion depth line of the constant properties model and suggestion model, (e) The comparison temperature distribution along with the insertion depth line of the constant properties model and suggestion model.

model, (e) The comparison temperature distribution along with the insertion depth line of the constant properties model and suggestion model.

This section demonstrated the effect of the property models suggestion, which is represented in section 5.3, compared with the constant properties model. The SAR and temperature differences can be observed in the tissue temperature exceeding 60 deg C, mainly could be clearly observed when the tissue exceeds 100 deg C. Moreover, the result is indicated the property functions that can more extensively affect the wider tissue area, as shown in Figs. 19(b) and 19(c). The consideration of tissue properties functions is essential to the SAR and temperature predicting in the liver tissue during the MWA treatment process.

6. Conclusions

This study proposed the effect of mainly property model types and characteristics of each property function on thermal response in the liver tissue during the MWA treatment process. The microwave power of 45 W and the microwave frequency of 2,45 GHz are considered for all cases. The main property model types as the constant properties model, Shao *et al*. model, Wang *et al*. model, and Xu *et al*. model are developed and investigated on the SAR distribution, tissue temperature distribution, and the fraction of necrotic tissue during the MWA process with same governing equations, initial conditions, and boundaries conditions. The mathematical models are developed under the couple with the electromagnetic wave propagation, heat transfer in the

biological tissue, and the Arrhenius damage equation. In order to verify the accuracy and precision of the presented numerical model, the numerical model of the constant properties is validated with the experimental results obtained by Yang *et al*.[15] under the same testing condition, as shown in section 5.1. The results demonstrate the difference in the SAR distribution, tissue temperature distribution, and the fraction of necrotic tissue when applied to the different properties model in the same conditions, as shown in section 5.2. However, this section cannot indicate the properties that cause the different results. So, section 5.3 demonstrated the effect of each property functions on the thermal response in the liver tissue during the MWA treatment process with the same power and frequency. These results show the distance tissue temperature when using the different property function. The electrical conductivity by Xu *et al*. is the most impact function, followed by the blood perfusion rate by Shao *et al*., relative permittivity by Wang *et al*., thermal conductivity by Shao *et al*., and specific heat capacity by Wang *et al*., respectively. In the last section, the prediction distribution of the suggestion property model is compared with the result of the constant properties model. The difference between the two models can be observed when tissue temperature exceeds 60 deg C, and it is clearly observed when tissue temperature exceeds 100 deg C. The main reason for the difference is that some functions consider the effect of tissue evaporation during the ablation process, but some properties are not considered. However, in some cases, the constant properties might be a good choice because it is simple and predicts fair results when applied in the tissue temperature not exceeding 100 deg C.

Acknowledgements

This study was supported by Thammasat Postdoctoral Fellowship, the Program Management Unit for Human Resources & Institutional Development, Research, and Innovation, NXPO (Grant Number B05F630092, B05F640205), Thailand Science Research and Innovation Fundamental Fund (TUFF41/2566), and National Research Council of Thailand (Grant Number N42A650197).

Conflict of Interest

There is no conflict of interest.

Supporting Information

Not applicable.

Appendix A. Dielectric properties of liver tissue, the relative permittivity (ε_r) and the electric conductivity (σ) by Wang *et al*. and Xu *et al*. models

The relative permittivity functions (ε_r)

$\varepsilon_{r,Wang}(T) = 47.043 - 0.042(T + 273.15)$ For 37 °C ≤ T ≤ 100 °C (A1)

$\varepsilon_{r,Wang}(T) = 5459.8 - 14.55(T + 273.15)$ For 100 °C ≤ T ≤ 101 °C (A2)

$\varepsilon_{r,Wang}(T) = 16.67101°C \leq T$ For 101 °C ≤ T (A3)

The electric conductivity (σ)

Wang *et al*.'s model

$\sigma_{Wang}(T) = 1.7381 - 0.0004(T + 273.15)$ For 37 °C ≤ T ≤ 100 °C (A4)

$\sigma_{Wang}(T) = 294.17 - 0.78(T + 273.15)$ For 100 °C ≤ T ≤ 101 °C (A5)

$\sigma_{Wang}(T) = 0.81$ For 101 °C ≤ T (A6)

Xu *et al*.'s model

$\sigma_{Xu}(T) = 1.7381 - 0.0004(T + 273.15)$ For 37 °C ≤ T ≤ 100 °C (A7)

$\sigma_{Xu}(T) = 2.173\left(1 - \frac{1}{1+exp(5.9506-0.0697T)}\right)$ For 100 °C < T (A8)

Appendix B. Blood perfusion rate (ω_b) and the thermal properties, i.e., thermal conductivity (k) and specific heat capacity (C_p) of the liver tissue by Shao *et al*., Wang *et al*., and Xu *et al*. models

Blood perfusion rate (ω_b)

Shao *et al*.'s model

$\omega_{b,Shao}(\Omega) = \omega_{b0}$ For Ω(T) ≤ 0 (B1)

$\omega_{b,Shao}(\Omega) = \omega_{b0}[1 + 25\Omega(T) - 260\Omega(T)^2]$ For 0 < Ω(T) ≤ 0.1 (B2)

$\omega_{b,Shao}(\Omega) = \omega_{b0}exp[-\Omega(T)]$ For 0.1 ≤ Ω(T) (B3)

where ω_b is the blood perfusion rate of liver tissue, ω_{b0} is the constant blood perfusion rate of liver tissue, and Ω(T) is the degree of tissue injury. In the normal liver, the ω_{b0} is 6.4 x 10^{-3} s^{-1}. In the study by Shao *et al*., liver tissue's blood perfusion rate depends on the degree of tissue injury. Although the degree of tissue injury is dependent on the tissue temperature, there are different blood perfusion rate values when considered by direct temperature and degree of tissue injury. This will be discussed in the next section.

Wang *et al*. model

$\omega_{b,Wang}(T) = 0.00035 + 0.000021(T + 273.15)$ (B4)

Xu *et al*. model

$\omega_b(T) = 0.016$ For 37°C ≤ T ≤ 60°C (B5)

$\omega_b(T) = 0$ For 60 < T (B6)

The thermal properties

Shao *et al*.'s model

$k_{Shao}(T) = k_{ref} + 0.0013 \times (T - T_{ref})$ For T ≤ 100 °C

$k_{Shao}(T) = k(100)$ For 100 °C < T

$C_{p,Shao}(T) = C_0$ For T ≤ 63.5°C

$C_{p,Shao}(T) = C_0 + C_1 \times (T - 63.5)$ For 63.5℃ < T

References

[1] T. Takayama, M. Makuuchi, S. Hirohashi, M. Sakamoto, J. Yamamoto, K. Shimada, T. Kosuge, S. Okada, K. Takayasu, S. Yamasaki, Early hepatocellular carcinoma as an entity with a high rate of surgical cure, *Hepatology*, 1998, **28**, 1241-1246, doi: 10.1002/hep.510280511.

[2] A. Dalia Ricci, A. Rizzo, C. Bonucci, S. Tavolari, A. Palloni, G. Frega, V. Mollica, N. Tober, E. Mazzotta, C. Felicani, C. Serra, G. Brandi, The (eternal) debate on microwave ablation Versus radiofrequency ablation in BCLC-a hepatocellular carcinoma, *In Vivo*, 2020, **34**, 3421-3429, doi: 10.21873/invivo.12181.

[3] T. Ryu, Y. Takami, Y. Wada, S. Sasaki, H. Saitsu, Predictive impact of the prognostic nutritional index in early-staged hepatocellular carcinoma after operative microwave ablation, *Asian Journal of Surgery*, 2022, **45**, 202-207, doi: 10.1016/j.asjsur.2021.04.043.

[4] P. Keangin, P. Rattanadecho, T. Wessapan, An analysis of heat transfer in liver tissue during microwave ablation using single and double slot antenna, *International Communications in Heat and Mass Transfer*, 2011, **38**, 757-766, doi: 10.1016/j.icheatmasstransfer.2011.03.027.

[5] P. Keangin, T. Wessapan, P. Rattanadecho, Analysis of heat transfer in deformed liver cancer modeling treated using a microwave coaxial antenna, *Applied Thermal Engineering*, 2011, **31**, 3243-3254, doi: 10.1016/j.applthermaleng.2011.06.005.

[6] EASL recommendations on treatment of hepatitis C_{2018}, *Journal of Hepatology*, 2018, **69**, 461-511, doi: 10.1016/j.jhep.2018.03.026.

[7] A. D. Strickland, P. J. Clegg, N. J. Cronin, B. Swift, M. Festing, K. P. West, G. M. Robertson, D. M. Lloyd, Experimental study of large-volume microwave ablation in the liver, *British Journal of Surgery*, 2002, **89**, 1003-1007, doi: 10.1046/j.1365-2168.2002.02155.x.

[8] A.U. Hines-Peralta, N. Pirani, P. Clegg, N. Cronin, T.P. Ryan, Z. Liu, and S.N. Goldberg, Microwave Ablation: Results with a 2.45-GHz Applicator in ex Vivo Bovine and in Vivo Porcine Liver, *Radiology-Radiological Society of North America*, 2006, **239**, 94-104, doi: 10.1148/radiol.2383050262.

[9] T. Wu, P. Li, Q. Shao, J. Hong, L. Yang, S. Wu, A simulation-experiment method to characterize the heat transfer in ex-vivo porcine hepatic tissue with a realistic microwave ablation system, *Numerical Heat Transfer, Part A: Applications*, 2013, **64**, 729-743, doi: 10.1080/10407782.2013.798202.

[10] P. Saccomandi, E. Schena, C. Massaroni, Y. Fong, R. F. Grasso, F. Giurazza, B. Beomonte Zobel, X. Buy, J. Palussiere, R. L. Cazzato, Temperature monitoring during microwave ablation in ex vivo porcine livers, *European Journal of Surgical Oncology (EJSO)*, 2015, **41**, 1699-1705, doi: 10.1016/j.ejso.2015.08.171.

[11] V. Lopresto, R. Pinto, L. Farina, M. Cavagnaro, Microwave thermal ablation: effects of tissue properties variations on predictive models for treatment planning, *Medical Engineering & Physics*, 2017, **46**, 63-70, doi: 10.1016/j.medengphy.2017.06.008.

[12] C. Marcelin, J. Leiner, S. Nasri, F. Petitpierre, Y. Le Bras, M. Yacoub, N. Grenier, J. C. Bernhard, F. Cornelis, In vivo percutaneous microwave ablation in kidneys: correlation with ex vivo data and ablation work, *Diagnostic and Interventional Imaging*, 2018, **99**, 3-8, doi: 10.1016/j.diii.2017.09.002.

[13] A. Z. Ibitoye, T. Orotoye, E. O. Nwoye, M. A. Aweda, Analysis of efficiency of different antennas for microwave ablation using simulation and experimental methods, *Egyptian Journal of Basic and Applied Sciences*, 2018, **5**, 24-30, doi: 10.1016/j.ejbas.2018.01.005.

[14] F. Hübner, R. Schreiner, C. Reimann, B. Bazrafshan, B. Kaltenbach, M. Schüßler, R. Jakoby, T. J. Vogl, Ex vivo validation of microwave thermal ablation simulation using different flow coefficients in the porcine liver, *Medical Engineering & Physics*, 2019, **66**, 56-64, doi: 10.1016/j.medengphy.2019.02.007.

[15] D. Yang, M. C. Converse, D. M. Mahvi, J. G. Webster, Expanding the bioheat equation to include tissue internal water evaporation during heating, *IEEE Transactions on Biomedical Engineering*, 2007, **54**, 1382-1388, doi: 10.1109/tbme.2007.890740.

[16] P. Rattanadecho, P. Keangin, Numerical study of heat transfer and blood flow in two-layered porous liver tissue during microwave ablation process using single and double slot antenna, *International Journal of Heat and Mass Transfer*, 2013, **58**, 457-470, doi: 10.1016/j.ijheatmasstransfer.2012.10.043.

[17] T. Wang, G. Zhao, B. Qiu, Theoretical evaluation of the treatment effectiveness of a novel coaxial multi-slot antenna for conformal microwave ablation of tumors, International *Journal of Heat and Mass Transfer*, 2015, **90**, 81-91, doi: 10.1016/j.ijheatmasstransfer.2015.06.030.

[18] C.L. Brace, Annual International Conference of the IEEE Engineering in Medicine and Biology Society, 2008, **30**, 230-233.

[19] Y. L. Shao, B. Arjun, H. L. Leo, K. J. Chua, Nano-assisted radiofrequency ablation of clinically extracted irregularly-shaped liver tumors, *Journal of Thermal Biology*, 2017, **66**, 101-113, doi: 10.1016/j.jtherbio.2017.04.005.

[20] M. Trujillo, E. Berjano, Review of the mathematical functions used to model the temperature dependence of electrical and thermal conductivities of biological tissue in radiofrequency ablation, *International Journal of Hyperthermia*, 2013, **29**, 590-597, doi: 10.3109/02656736.2013.807438.

[21] I. dos Santos, D. Haemmerich, D. Schutt, A. F. da Rocha, L. R. Menezes, Probabilistic finite element analysis of radiofrequency liver ablation using the unscented transform, *Physics in Medicine and Biology*, 2009, **54**, 627-640, doi: 10.1088/0031-9155/54/3/010.

[22] Y. Xu, M. A. J. Moser, E. Zhang, W. Zhang, B. Zhang, Large and round ablation zones with microwave ablation: a preliminary study of an optimal aperiodic tri-slot coaxial antenna with the π-matching network section, *International Journal of Thermal Sciences*, 2019, **140**, 539-548, doi: 10.1016/j.ijthermalsci.2019.03.022.

[23] Z. Ji, C. L. Brace, Expanded modeling of temperature-dependent dielectric properties for microwave thermal ablation, *Physics in Medicine and Biology*, 2011, **56**, 5249-5264, doi:

10.1088/0031-9155/56/16/011.
[24] J. Sebek, N. Albin, R. Bortel, B. Natarajan, P. Prakash, Sensitivity of microwave ablation models to tissue biophysical properties: a first step toward probabilistic modeling and treatment planning, *Medical Physics*, 2016, **43**, 2649-2661, doi: 10.1118/1.4947482.
[25] P. Keangin, P. Rattanadecho, Analysis of heat transport on local thermal non-equilibrium in porous liver during microwave ablation, *International Journal of Heat and Mass Transfer*, 2013, **67**, 46-60, doi: 10.1016/j.ijheatmasstransfer.2013.07.064.
[26] J. M. Bertram, D. Yang, M. C. Converse, J. G. Webster, D. M. Mahvi, Antenna design for microwave hepatic ablation using an axisymmetric electromagnetic model, *BioMedical Engineering OnLine*, 2006, **5**, 15, doi: 10.1186/1475-925x-5-15.
[27] H. H. Pennes, Analysis of tissue and arterial blood temperatures in the resting human forearm, *Journal of Applied Physiology*, 1948, **1**, 93-122, doi: 10.1152/jappl.1948.1.2.93.
[28] F.C. Henriques Jr, and A. R. Moritz, Studies of thermal injury: i. the conduction of heat to and through skin and the temperatures attained therein. a theoretical and an experimental investigation, *The American Journal of Pathology*, 1947, **23**, 530.
[29] S. K. Hall, E. H. Ooi, S. J. Payne, Cell death, perfusion and electrical parameters are critical in models of hepatic radiofrequency ablation, *International Journal of Hyperthermia*, 2015, **31**, 538-550, doi: 10.3109/02656736.2015.1032370.